Metabolism 158 (2024) 155976

Contents lists available at ScienceDirect

Metabolism

journal homepage: www.journals.elsevier.com/metabolism

Estrogen receptor-α signaling in tanycytes lies at the crossroads of fertility and metabolism

Daniela Fernandois [a], Mariam Rusidzé [b], Helge Mueller-Fielitz [c], Florent Sauve [a], Eleonora Deligia [a], Mauro S.B. Silva [a], Florence Evrard [a], Aurelio Franco-García [d], Daniele Mazur [a], Ines Martinez-Corral [a], Nathalie Jouy [e], S. Rasika [a], Claude-Alain Maurage [a], Paolo Giacobini [a], Ruben Nogueiras [f], Benedicte Dehouck [a], Markus Schwaninger [c], Francoise Lenfant [b], Vincent Prevot [a,*]

[a] *Univ. Lille, Inserm, CHU Lille, Laboratory of Development and Plasticity of the Neuroendocrine Brain, Lille Neuroscience & Cognition, UMR-S1172, EGID, DISTALZ, F-59000 Lille, France*
[b] *Institute of Metabolic and Cardiovascular Diseases (I2MC) Equipe 4, Inserm U1297UPS, CHU, Toulouse, France*
[c] *Institute of Experimental and Clinical Pharmacology and Toxicology, Center of Brain, Behavior and Metabolism, University of Lübeck, Lübeck, Germany*
[d] *Group of Cellular and Molecular Pharmacology, Department of Pharmacology, CEIR Campus Mare Nostrum, University of Murcia, Spain, Instituto Murciano de Investigación Biosanitaria (IMIB), Pascual Parrilla, Murcia, Spain*
[e] *PLBS UAR 2014 – US41, France*
[f] *CIMUS, Universidade de Santiago de Compostela-Instituto de Investigación Sanitaria, Santiago de Compostela 15782, Spain- CIBER Fisiopatología de la Obesidad y Nutrición (CIBERobn), 15706, Spain*

ARTICLE INFO

Keywords:
Estrogens
Tanycytes
LH pulsatility
Female metabolism
Reproduction
Hypothalamus

ABSTRACT

Background: Estrogen secretion by the ovaries regulates the hypothalamic-pituitary-gonadal axis during the reproductive cycle, influencing gonadotropin-releasing hormone (GnRH) and luteinizing hormone (LH) secretion, and also plays a role in regulating metabolism. Here, we establish that hypothalamic tanycytes—specialized glia lining the floor and walls of the third ventricle—integrate estrogenic feedback signals from the gonads and couple reproduction with metabolism by relaying this information to orexigenic neuropeptide Y (NPY) neurons.
Methods: Using mouse models, including mice floxed for *Esr1* (encoding estrogen receptor alpha, ERα) and those with Cre-dependent expression of designer receptors exclusively activated by designer drugs (DREADDs), along with viral-mediated, pharmacological and indirect calorimetric approaches, we evaluated the role of tanycytes and tanycytic estrogen signaling in pulsatile LH secretion, cFos expression in NPY neurons, estrous cyclicity, body-weight changes and metabolic parameters in adult females.
Results: In ovariectomized mice, chemogenetic activation of tanycytes significantly reduced LH pulsatile release, mimicking the effects of direct NPY neuron activation. In intact mice, tanycytes were crucial for the estrogen-mediated control of GnRH/LH release, with tanycytic ERα activation suppressing fasting-induced NPY neuron activation. Selective knockout of *Esr1* in tanycytes altered estrous cyclicity and fertility in female mice and affected estrogen's ability to inhibit refeeding in fasting mice. The absence of ERα signaling in tanycytes increased *Npy* transcripts and body weight in intact mice and prevented the estrogen-mediated decrease in food intake as well as increase in energy expenditure and fatty acid oxidation in ovariectomized mice.
Conclusions: Our findings underscore the pivotal role of tanycytes in the neuroendocrine coupling of reproduction and metabolism, with potential implications for its age-related deregulation after menopause.
Significance statement: Our investigation reveals that tanycytes, specialized glial cells in the brain, are key interpreters of estrogen signals for orexigenic NPY neurons in the hypothalamus. Disrupting tanycytic estrogen receptors not only alters fertility in female mice but also impairs the ability of estrogens to suppress appetite. This work thus sheds light on the critical role played by tanycytes in bridging the hormonal regulation of cyclic reproductive function and appetite/feeding behavior. This understanding may have potential implications for age-related metabolic deregulation after menopause.

* Corresponding author at: Inserm U1172, Bâtiment Biserte, Place de Verdun, 59045 Lille Cedex, France.
E-mail address: vincent.prevot@inserm.fr (V. Prevot).

https://doi.org/10.1016/j.metabol.2024.155976
Received 28 March 2024; Accepted 12 July 2024
Available online 15 July 2024

1. Introduction

The keystone of the hypothalamic-pituitary-gonadal (HPG) or reproductive axis is gonadotropin-releasing hormone (GnRH). Hypothalamic neurons producing GnRH release this neurohormone into the pituitary portal circulation at the median eminence of the hypothalamus, from where it travels to the anterior pituitary to stimulate the secretion of the gonadotropins, luteinizing hormone (LH) and follicle-stimulating hormone (FSH). These in turn act on the ovaries and testes, leading to the production of sex steroid hormones and gametogenesis [1]. However, GnRH is not released uniformly but in a specific pattern that is essential to its function, featuring low-level basal secretion with superimposed pulsatile rhythms [2–4]. In mammals, including humans, each GnRH pulse in the portal circulation drives an LH pulse in the general circulation [5–8], and their frequency appears to be tightly regulated across the estrous cycle by the fluctuating levels of gonadal hormones, including estrogens in females [9,10]. Gonadectomy relieves this restraint, increasing the frequency of LH pulses, whereas exogenous 17β-estradiol (E_2) supplementation restores LH frequency to intact diestrus levels [10].

Estrogen sensing through the estrogen receptor (ER) α is essential to this process. However, GnRH neurons do not themselves express ERα. Instead, the feedback effects of estrogens on GnRH/LH release are thought to be mediated by other estrogen-sensitive neurons of the GnRH network [11–17]. Even though the involvement of ERα-expressing kisspeptin neurons in the arcuate nucleus of the hypothalamus (ARH), known to control GnRH pulsatile release [18], in this process has been a matter of debate during this last decade [12,19], a 2022 study convincingly showed by the selective knockout of *Esr1*, the gene coding ERα, in >80 % of adult ARH kisspeptin neurons that the estrogen negative feedback control of LH secretion is indeed primarily achieved through the *Esr1*-dependent modulation of ARH kisspeptin neurons [20]. Interestingly, the ARH is also home to other neural networks, such as those involved in the control of energy homeostasis, and appetite-promoting ARH neurons that express neuropeptide Y (NPY) and agouti-related protein (AgRP) are known to robustly influence GnRH/LH pulsatile release [21,22] and have direct inhibitory synaptic connections with kisspeptin neurons [23]. Intriguingly, LH pulsatility, which is increased in ovariectomized mice, *i.e.* when the gonadal source of E_2 is removed, is slowed down by the acute and selective chemogenetic activation of NPY neurons [24] or treatment with NPY [25], even though these neurons too do not appear to express ERα [26]. How then are the anorexigenic effects of estrogen across the estrous cycle integrated and relayed to GnRH neurons?

In addition to neurons of the GnRH network, GnRH release is also controlled by peculiar hypothalamic ependymoglial cells called tanycytes, which stretch from their cell bodies lining the walls and floor of the third ventricle (3 V) to their "endfeet" that contact the pituitary portal circulation at the median eminence [27]. Early studies have suggested that tanycytes accumulate radiolabeled 17β-estradiol [28], express estrogen receptors [29], and respond to estrogens *in vitro* [30]. However, the physiological relevance of estradiol signaling in tanycytes *in vivo* remains unknown. Interestingly, we and others have recently shown that tanycytes also tightly modulate the activity of appetite-controlling neurons of the ARH [31,32]. We therefore asked whether the sensing of estrogens by tanycytes could play an active role in controlling GnRH/LH basal and pulsatile release or conveying estrogen-weighted information to metabolic circuits in the ARH.

2. Results

2.1. Hypothalamic tanycytes mediate GnRH/LH pulsatility regulation by arcuate neurons

To determine whether tanycytic input is involved in the modulation of GnRH/LH pulsatility by NPY/AgRP neurons, we first chemogenetically activated tanycytes in ovariectomized mice using designer receptors exclusively activated by designer drugs (DREADD), an approach we have previously used to study their function [33]. We selectively expressed $hM3D_{Gq}$ in tanycytes *via* the stereotaxic injection of an AAV1/2 vector expressing the Cre recombinase under the control of the tanycyte-specific human deiodinase 2 (Dio2) promoter into the lateral ventricle of a mouse line in which an activator DREADD, $hM3D_{Gq}$, can be expressed in a Cre-dependent manner [34] with the $hM3D_{Gq}$ activator clozapine-N-oxide (CNO; 1 mg/kg, i.p.) (Fig. 1A). As evidenced by the expression of GFP from an internal ribosomal entry site (IRES) downstream of $hM3D_{Gq}$ [34], genetic recombination was selectively induced in tanycytes ($hM3D_{Gq}^{Tanycytes}$ mice) (Fig. 1B). Mice were then subjected to bilateral ovariectomy (Fig. 1A). Iterative blood sampling every 6 min before CNO treatment showed the expected increase in spontaneous LH pulse frequency and basal release after ovariectomy (Fig. 1C) when compared to intact cycling mice [10]. The LH pulse frequency was dramatically reduced following the activation of tanycytes by CNO (Fig. 1C-E), mimicking the previously reported effects of selectively activating NPY/AgRP neurons [24].

To gain further insight into the underlying communication between tanycytes and ARH neurons, we then assessed cFos expression as a proxy for cellular activation in the presence or absence of CNO treatment in ovariectomized $hM3D_{Gq}^{Tanycytes}$ mice. While $hM3D_{Gq}$ appeared to be expressed in almost all tanycytes (Fig. 1B), CNO, 30 min after its injection, only triggered cFos expression in tanycytes lining the walls of the 3 V adjacent to the ARH (Fig. 1F, white arrows), but not those lining the median eminence (Fig. 1F, pink arrows). Many ARH neurons in contact with GFP-immunofluorescent tanycytic processes also displayed enhanced cFos expression (Fig. 1F, yellow arrows). Similarly, as visualized using the highly sensitive RNAscope fluorescent *in situ* hybridization approach, CNO induced *Fos* mRNA expression in both ARH tanycytes and ARH neurons (Fig. 1G). To verify the identity of these neurons, we investigated the colocalization of *Fos* and *Npy* transcripts in ovariectomized $hM3D_{Gq}^{Tanycytes}$ mice treated with CNO or 0.9 % NaCl. While only ~4 % of *Npy*-expressing neurons were seen to express *Fos* transcripts in vehicle-treated mice, CNO increased this proportion 3-fold (Fig. 1G–I). This CNO-induced tanycyte-mediated increase in NPY *Fos* expression was associated with a marked increase in food intake (Supplementary Fig. 1). These results show that tanycytes are not only integral components of the feedback loop by which the gonads restrain GnRH/LH pulsatile release, but that in the absence of estrogen feedback, the activation of ARH tanycytes in ovariectomized mice leads to the increased activation of orexigenic NPY neurons.

2.2. ERα is expressed in female tanycytes

Because estrogens are the main gonadal effectors controlling GnRH/LH pulsatility, we next verified whether tanycytes have the necessary estrogen-sensing equipment to play a role in this process. We looked for mRNA for *Esr1*, which encodes ERα, in the tuberal region of the hypothalamus of female mice in estrus using RNAscope technology. While *Esr1* mRNA expression was abundant in putative neurons of the ARH, it could also be visualized in the cell bodies of vimentin-immunoreactive tanycytes lining the walls and the floor of the 3 V (Fig. 2A). To investigate ERα expression dynamics in tanycytes during the estrous cycle, we performed fluorescence-activated cell sorting (FACS) on tanycytes expressing the fluorescent reporter tdTomato upon Cre-mediated recombination (Fig. 2B) using either recombinant TAT-Cre protein infusion into the 3V or AVV1/2-Dio2::Cre infection of $tdTomato^{loxP\text{-}STOP\text{-}loxP}$ mice (Supplementary Fig. 2A, B). Subsequent qRT-PCR analyses revealed that tanycytes expressed low levels of *Esr2* transcripts coding for ERβ (Fig. 2C). In contrast, they abundantly expressed *Esr1* mRNA, with levels varying across the estrous cycle and peaking in estrus, when estrogens reach nadir levels (Fig. 2C, D). Finally, to determine whether the proportion of tanycytes expressing the ERα protein was also changing during the estrous cycle, we performed dual FACS sorting

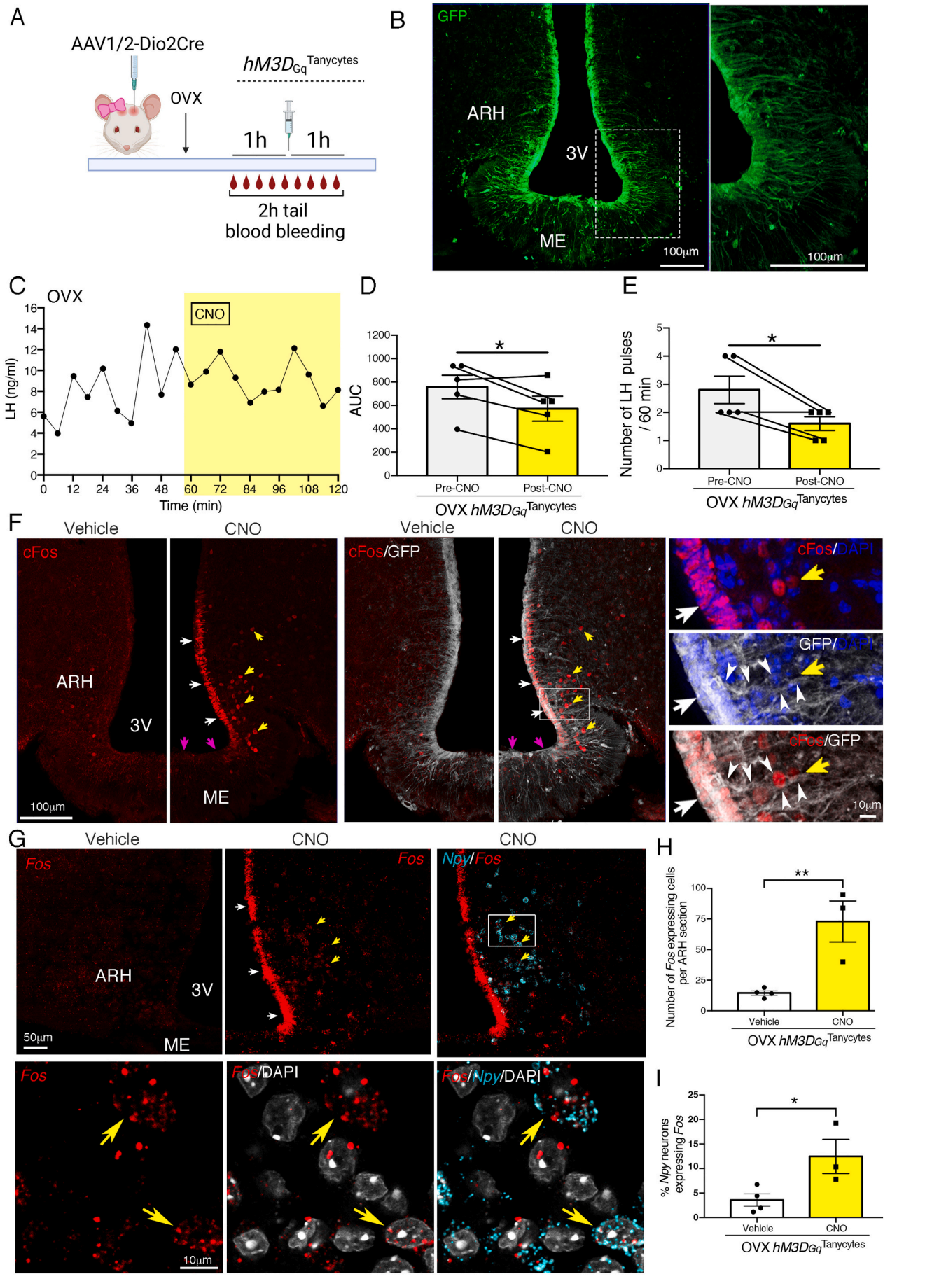

(caption on next page)

Fig. 1. Chemogenetic activation of tanycytes slows down ovariectomy-mediated acceleration of pulsatile LH release and activates arcuate Npy neurons. (A) Protocol for the iterative tail-blood sampling in mice, (B) expression of GFP in tanycytes as a reflection of $hM3D_{Gq}$ receptor expression in $hM3D_{Gq}^{Tanycytes}$ mice. *Right panel*, higher magnification of the framed region in the left panel. (C) Representative pulsatile LH release in bilaterally ovariectomized (OVX) $hM3D_{Gq}^{Tanycytes}$ mice 1 h before and after i.p. clozapine-N-oxide (CNO; 1 mg/kg) administration, (D) area under the curve of LH and (E) LH pulse frequency before (grey bars) and after (yellow bars) 1 mg/kg CNO i.p. injection in OVX $hM3D_{Gq}^{Tanycytes}$. (F) Immunofluorescence of OVX $hM3D_{Gq}^{Tanycytes}$ mice brains 30 min after vehicle (VH) or CNO i.p. administration. White arrows indicate the arcuate nucleus of the hypothalamus (ARH) tanycytes, pink arrows indicate median eminence tanycytes and yellow arrows indicate cells immunoreactive for cFOS in the proximity of tanycytic processes within the ARH. cFos positive immunolabeling is observed in red, GFP (representative of $hM3D_{Gq}$ expression) in white and DAPI in blue as nuclear counterstaining. (G) Fluorescent *in situ* hybridization of OVX $hM3D_{Gq}^{Tanycytes}$ brain mice for *Fos* (red dots), *Npy* (cyan dots), and DAPI (white) 30 min after CNO i.p. injection. White arrows indicate *Fos* expression in tanycytes and yellow arrows indicate *Fos* expression in NPY neurons. (H) Number of cells positive for *Fos* within the ARH nucleus, (I) Percentage of *Npy* neurons positive for *Fos* within the ARH nucleus. Vehicle $N = 4$ and CNO $N = 3$. Graphs are plotted as Mean ± SEM. Statistical differences were determined by a paired two-sided Student's *t*-test (D and E) or an unpaired two-sided Student's *t*-test (H and I). $^{*}p < 0.05$, $^{**}p < 0.01$. (For interpretation of the references to colour in this figure legend, the reader is referred to the web version of this article.)

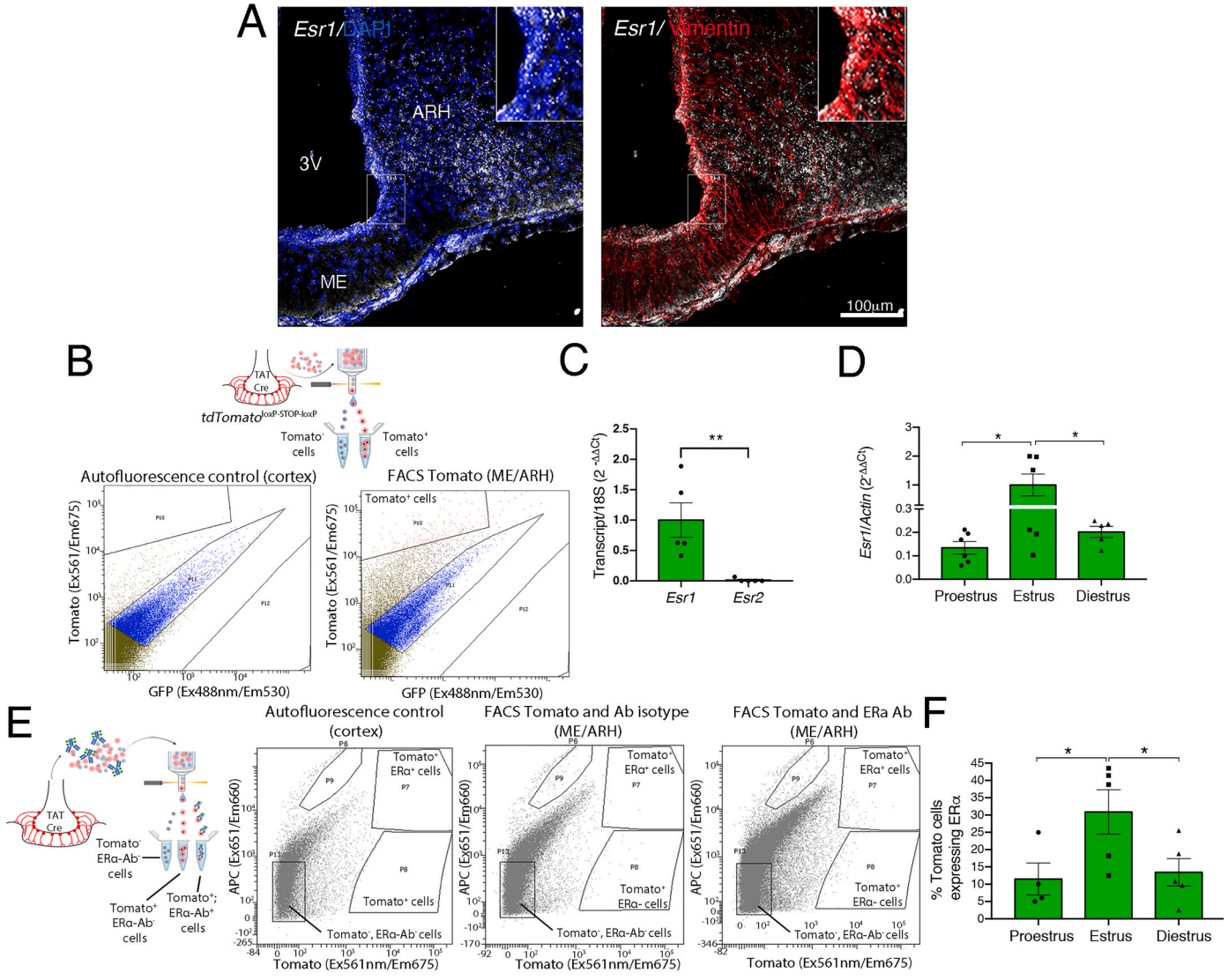

Fig. 2. *Esr1* transcripts are expressed in tanycytes in female mice. (A) Fluorescent *in situ* hybridization for *Esr1* in the brain of $Esr1^{loxP/loxP}$ mice. White dots show *Esr1* transcripts and the red labelling shows immunoreactivity for vimentin, which is a marker for tanycytes. (B) Representative diagram of the design of the fluorescent activated cell sorting (FACS) experiment and dot-plots showing the tissue autofluorescence control and the gating strategy for cell sorting in the median eminence (ME)/arcuate nucleus of the hypothalamus (ARH) region. (C) Real-time qPCR for *Esr1* coding ERα and *Esr2* coding ERβ in tanycytes isolated by FACS from estrus td$Tomato^{Tanycytes}$ female mice, $N = 5$. (D) Real-time qPCR for *Esr1* in FACS-isolated tanycytes at different stages of the estrous cycle; Proestrus ($N = 6$), Estrus (N = 6) and Diestrus (N = 5). (E) Representative diagram of the design of the FACS experiment and dot-plots showing the tissue autofluorescence and antibody isotype controls and the gating strategy for cell sorting in the ME/ARH. (F) Percentage of tomato-positive tanycytes expressing ERα-immunoreactivity during the different stages of the estrous cycle; Proestrus (N = 4), Estrus (N = 5) and Diestrus (N = 5). B Bars are shown as Mean ± SEM. Statistical differences were determined by an unpaired two-sided Student's *t*-test (C) or a one-way ANOVA (normal data and homogeneity of variances) followed by test Fisher's LSD test (D and F). $^{*}p < 0{,}05$ and $^{**}p < 0{,}01$. (For interpretation of the references to colour in this figure legend, the reader is referred to the web version of this article.)

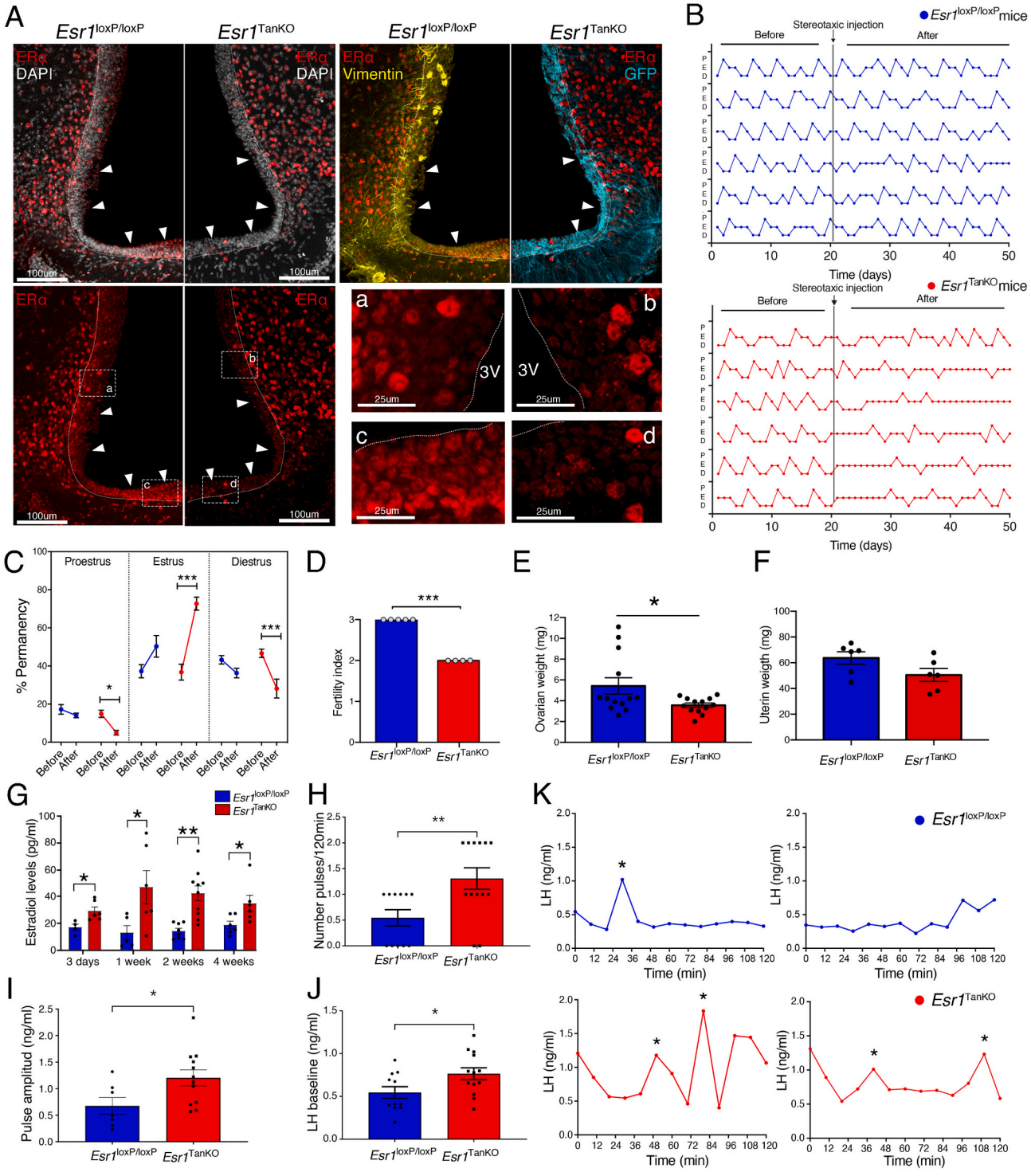

Fig. 3. Selective impairment of ERα production in adult tanycytes alters female fertility. (A) Immunoreactivity for ERα (shown in red) in *Esr1*$^{loxP/loxP}$ and *Esr1*^{TanKO} mouse littermates. Nuclei were labelled with DAPI (white). *Esr1*$^{loxP/loxP}$; *Rosa*^{mTmG} mice were injected into the lateral ventricle with an AAV1/2 expressing Dio2::gfp (*Esr1*$^{loxP/loxP}$) or Dio2::Cre (*Esr1*^{TanKO}). White arrowheads indicate the cell bodies of the tanycytic layer bordering the floor and the ventral wall of the third ventricle. Vimentin immunoreactivity is shown in yellow and cre-mediated membrane GFP expression in blue. a-d Subpanels depict higher magnification of the framed regions in the corresponding left panel. (B) Estrous cyclicity in females before and after stereotaxic surgery in *Esr1*$^{loxP/loxP}$ and *Esr1*^{TanKO} mice. (C) Percentage of permanency in proestrus, estrus, or diestrus of each mouse before and after mock (*Esr1*$^{loxP/loxP}$) or Cre-mediated genetic recombination in the *Esr1* gene (*Esr1*^{TanKO}) in tanycytes. *Esr1*$^{loxP/loxP}$ $N = 11$ and *Esr1*^{TanKO} $N = 12$. (D–F) Fertility index (D), ovarian weight (E) and uterine weight (F) at estrous in *Esr1*$^{loxP/loxP}$ and Esr1^{TanKO} littermates one month after genetic recombination. (G) Plasmatic levels of 17β-estradiol in *Esr1*$^{loxP/loxP}$ and *Esr1*^{TanKO} mice at different time points after mock or cre-mediated genetic recombination. (H-J) Mean pulse frequency (H), pulse amplitude (I), and basal levels of LH release (J). N = 12 for *Esr1*^{Wt} and $N = 13$ for *Esr1*^{TanKO} mice. (K) Representative figure of LH secretion observed for 2 h in intact *Esr1*^{Wt} (blue, K) and *Esr1*^{TanKO} (red, K) littermates. Bars are shown as Mean ± SEM. Statistical differences were determined by paired (C) and unpaired two-sided Student's *t*-tests (D-F and H-J) or a two-way ANOVA (normal data and homogeneity of variances) followed by test Fisher's LSD test (G). *p < 0,05, **p < 0,01 and **$p < 0.001$. (For interpretation of the references to colour in this figure legend, the reader is referred to the web version of this article.)

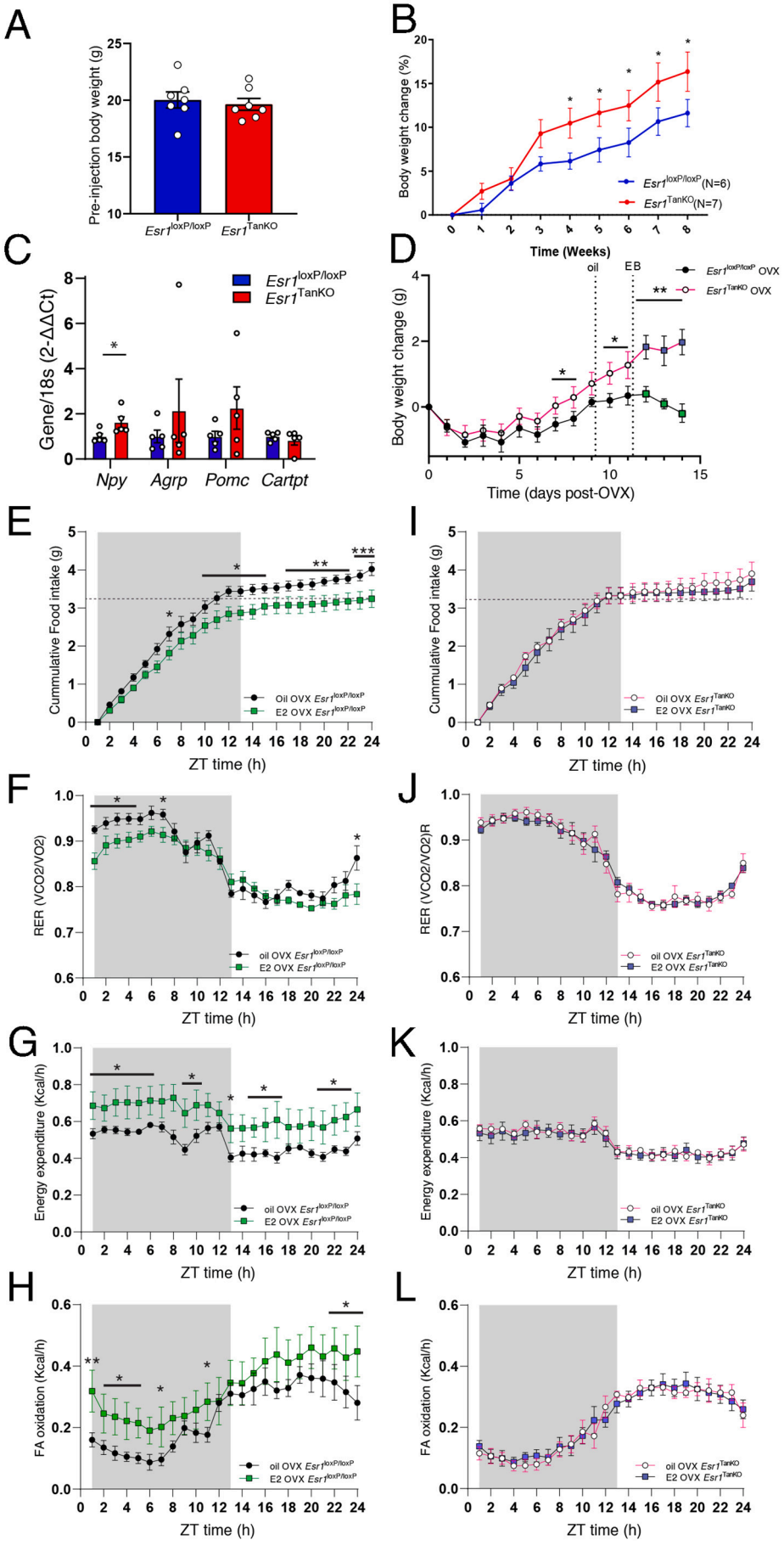

(caption on next page)

Fig. 4. ERα deletion in tanycytes produces hypothalamic insensitivity to estradiol. (A) Body weight distribution of *Esr1*$^{loxP/loxP}$ and *Esr1*^{TanKO} mice before the stereotaxic injection. (B) Percentage of body weight change after a vehicle (*Esr1*$^{loxP/loxP}$, N = 6) or Tat-Cre (*Esr1*^{TanKO}, *N* = 7) injection into the third ventricle of intact female mice. (C) Relative transcript levels in the mediobasal hypothalamus of estrous *Esr1*$^{loxP/loxP}$ and *Esr1*^{TanKO} female mice, N = 5 for each group. (D) Body weight change after OVX before (day 0–9) and after a daily subcutaneous injection of sesame oil (day 10–11) or estradiol benzoate (day 12–14) (N = 5 for *Esr1*$^{loxP/loxP}$ and N = 6 for *Esr1*^{TanKO}). (E,I) 24 h cumulative food intake for *Esr1*$^{loxP/loxP}$ (E) and *Esr1*^{TanKO} (I) mice. (F, J) 24-h respiratory exchange ratio, RER *Esr1*$^{loxP/loxP}$ (F) and *Esr1*^{TanKO} (J) littermates. (G, K) 24-h Energy expenditure for *Esr1*$^{loxP/loxP}$ (G) and *Esr1*^{TanKO} (K) animals. (*H*,*L*) 24-h Fatty acid oxidation for *Esr1*$^{loxP/loxP}$ (H) and *Esr1*^{TanKO} (L) mice. (*E*-H) *Esr1*$^{loxP/loxP}$ N = 5 and (I-L) *Esr1*^{TanKO} *N* = 6. Bars are shown as Mean ± SEM. Statistical differences were determined by an unpaired two-sided Student's t-tests (A, C) and a one-way ANOVA (normal data and homogeneity of variances) followed by test Fisher's LSD test (B, D-L). *p < 0,05, **p < 0,01 and ***p < 0,001.

combining the red fluorescent signal from the tdTomato reporter with the λ647 fluorescence of a secondary antibody detecting the primary antibody against ERα (Fig. 2E). Results showed an increased percentage of tanycytes expressing ERα immunoreactivity during estrus compared to other stages of the estrous cycle (Fig. 2F).

2.3. Knocking out Esr1 in tanycytes alters fertility in female mice

ERα protein could be clearly visualized by immunofluorescence in the nuclei of tanycytes and putative ARH neurons in the tuberal region of the hypothalamus of wildtype female mice in estrus (Fig. 3A), even though, as for *ERS1* transcript levels (Supplementary Fig. 2C), the ERα immunoreactive signal was seen to be lower in tanycytes than in neurons (Fig. 3A). As expected, however, ERα immunoreactivity was absent in NPY neurons (Supplementary Fig. 3 and Supplementary Movie 1). Selectively knocking out *Esr1* expression in tanycytes using the aforementioned Cre-mediated approaches in the *Esr1*$^{loxP/loxP}$ mice carrying the *Rosa*$^{mT/mG}$ reporter (*Esr1*^{TanKO} mice) efficiently dampened ERα immunoreactivity in cell nuclei lining the ventricular wall (Fig. 3A) and *Esr1* transcripts in FACS-isolated tanycytes (Supplementary Fig. 2D). This selective impairment of ERα production in tanycytes dramatically and permanently altered estrous cyclicity, with mice spending more time in estrus (Fig. 3B, C), and resulting in a decreased ability to produce litters over a 75-day period (Fig. 3D), even though the number of pups per litter, sex ratio, and survival rate of pups were unchanged (Supplementary Fig. 4A-C). One month after Cre-mediated genetic recombination, *Esr1*^{TanKO} mice during estrus showed decreased ovarian weight (Fig. 3E), but unaltered uterine weight (Fig. 3F), a physiological index of circulating estrogen levels. In agreement with these results, circulating levels of estrogens were seen to be permanently elevated starting shortly after Cre-mediated genetic recombination (Fig. 3G). This was accompanied by a modification in the size and distribution of antral follicles (Supplementary Fig. 4D, E) without any change in the total number of follicles between *Esr1*^{TanKO} and *Esr1*$^{loxP/loxP}$ littermates (Supplementary Fig. 4F-K).

Further supporting the idea that ARH tanycytes could be involved in mediating estrogen negative feedback effects on GnRH pulsatile release, the selective invalidation of ERα production in tanycytes not only increased LH pulse frequency (Fig. 3H, K) and amplitude (Fig. 3I, K), but also affected basal LH levels (Fig. 3J). While the increase in pulsatility might be explained, at least in part, by an alteration in communication between tanycytes and ARH neurons, the heightened baseline could be linked to an increased ability of GnRH neurons to release their neurohormone into the pituitary portal vasculature. Indeed, the latter phenomenon is regulated by the structural remodeling of the endfeet of median eminence tanycytes, which ensheathe GnRH neuronal terminals in the external zone of the median eminence and control the periodic access of these terminals to the pericapillary space of the pituitary portal blood vessels [35]; the permanent retraction of these endfeet thus leads to increased LH release and constant estrus in mice [36]. Keeping this in mind, we next performed electron microscopic studies of the median eminence of *Esr1*$^{loxP/loxP}$ and *Esr1*^{TanKO} littermates, using 18 nm gold-particle labeling to visualize GnRH-immunoreactive nerve terminals. Quantitative analyses showed that in *Esr1*^{TanKO} mice at estrus, there was a marked advance of GnRH axon terminals towards the pericapillary space when compared to their control littermates (Supplementary Fig. 4L, M), at levels comparable to those seen in ovariectomized *Esr1*$^{loxP/loxP}$ littermates (Supplementary Fig. 4L). In addition, GnRH neuronal terminals were frequently in direct apposition to the brain basement membrane delimiting the pericapillary space in *Esr1*^{TanKO} mice at estrus, a phenomenon never observed in *Esr1*$^{loxP/loxP}$ mice in the same phase (Supplementary Fig. 4M) and known to be associated with increased GnRH release [35,36]. Altogether, these data collectively suggest that tanycytes, through their sensing of estradiol, play a role in controlling both the pulsatile pattern and the basal level of GnRH release.

2.4. Knocking out Esr1 in tanycytes alters energy homeostasis in female mice

Estrogens play a crucial role in regulating body composition in women by reducing food intake, increasing fatty acid oxidation, and enhancing energy expenditure through ERα [37]. Consistent with this, the deletion of ERα in *Esr1*^{TanKO} mice leads to increased body weight gain in intact females as early as 3 weeks after Cre-mediated recombination in tanycytes (Fig. 4A, B). This weight gain is accompanied by a specific rise in NPY mRNA expression in the mediobasal hypothalamus of *Esr1*^{TanKO} mice (Fig. 4C). Notably, this increase in body weight gain persists even after ovariectomy in *Esr1*^{TanKO} mice (Fig. 4D), mimicking menopause in women. Since estrogens are known to suppress NPY expression while increasing energy expenditure and fatty acid oxidation [38,39], we investigated whether *Esr1*^{TanKO} mice developed a central insensitivity to estrogenic actions by administering a daily injection of estradiol benzoate for 3 days to ovariectomized *Esr1*$^{loxP/loxP}$ and *Esr1*^{TanKO} littermates. Estradiol benzoate promptly reduced body weight gain in *Esr1*$^{loxP/loxP}$ mice, but not in the *Esr1*^{TanKO} littermates (Fig. 4D). Additionally, estradiol benzoate effectively reduced food intake and the respiratory exchange ratio (RER), and increased energy expenditure and fatty acid oxidation in *Esr1*$^{loxP/loxP}$ mice (Fig. 4E-H). These effects were absent in *Esr1*^{TanKO} mice (Fig. 4I-L). These experiments collectively demonstrate that ERα signaling in tanycytes is vital for maintaining hypothalamic estrogen sensitivity in the context of energy homeostasis.

2.5. ERα in tanycytes links estrogen signaling to appetite and fertility in cycling females

Next, to investigate whether tanycytes could be the missing link through which estrogens exert their anorexigenic effect by inhibiting NPY neurons, which themselves lack ERα, we treated intact (non-ovariectomized) female mice with either vehicle (DMSO) or the specific ERα agonist 4,4′,4″-(4-Propyl-[1H]-pyrazole-1,3,5-triyl)trisphenol (PPT, 3.5 mg/kg/12 h subcutaneously) [40] in the presence or selective absence of ERα in tanycytes. This treatment was administered at lights-off in female mice either fed *ad libitum* or subjected to overnight fasting, and food intake was measured on the morning of the next day or every hour for 10 h after refeeding at lights-on, respectively. As described previously for 17β-estradiol [26], PPT induced a pronounced reduction in food intake in control mice both during the fed state (Fig. 5A) and after refeeding in 12 h-fasting mice (Fig. 5B). The anorexigenic effect of PPT was blunted in littermates lacking ERα in tanycytes (Fig. 5A, B).

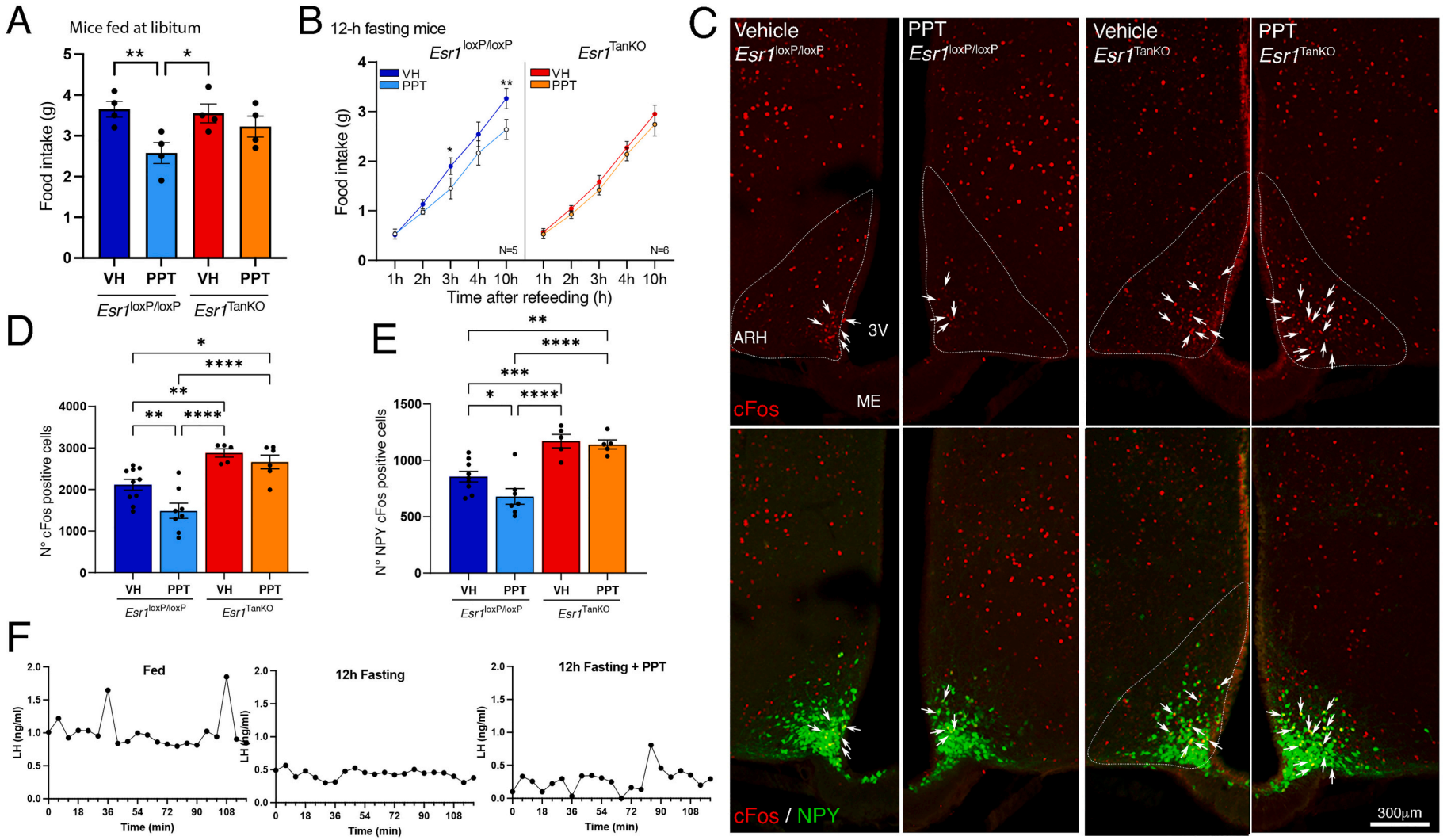

Fig. 5. Estrogen receptor α expression in female tanycytes is required for estrogens to exert its anorexigenic effect and fasting-induced cFos expression in NPY neurons. (A) Food intake after overnight *ad libitum* feeding in female *Esr1*$^{loxP/loxP}$ and *Esr1*^{tanKO} littermates treated or not with the ERα agonist PPT at lights off (N = 4 per group). (B) Hourly food intake at refeeding after overnight fasting (12 h) in female *Esr1*$^{loxP/loxP}$ (N = 5) and *Esr1*^{TanKO} (N = 6) littermates treated or not with the ERα agonist PPT at lights off. (C) cFos expression in the tuberal region of the hypothalamus after overnight fasting in *Npy*::*Gfp*;*Esr1*$^{loxP/loxP}$ and *Npy*::*Gfp*;*Esr1*^{TanKO} littermates treated with DMSO (vehicle, VH) or PPT. White arrows show GFP-fluorescent NPY neurons expressing cFOS. (D) Total number of cFOS-positive cells in the arcuate nucleus of the hypothalamus (ARH), and (E) Number of cFOS-positive GFP-expressing NPY neurons in the ARH after overnight fasting in *Npy*::*Gfp*;*Esr1*$^{loxP/loxP}$ and *Npy*::*Gfp*;*Esr1*^{TanKO} littermates treated with DMSO or PPT. (F) LH pulsatility in diestrous mice fed *ad libitum* or after overnight fasting (12 h) in the absence or presence of PPT treatment. Bars are shown as Mean ± SEM. Statistical differences were determined by a one-way ANOVA (normal data and homogeneity of variances) followed by test Fisher's LSD test (A,B, D and E). *p < 0,05, **p < 0,01 and ***p < 0,001.

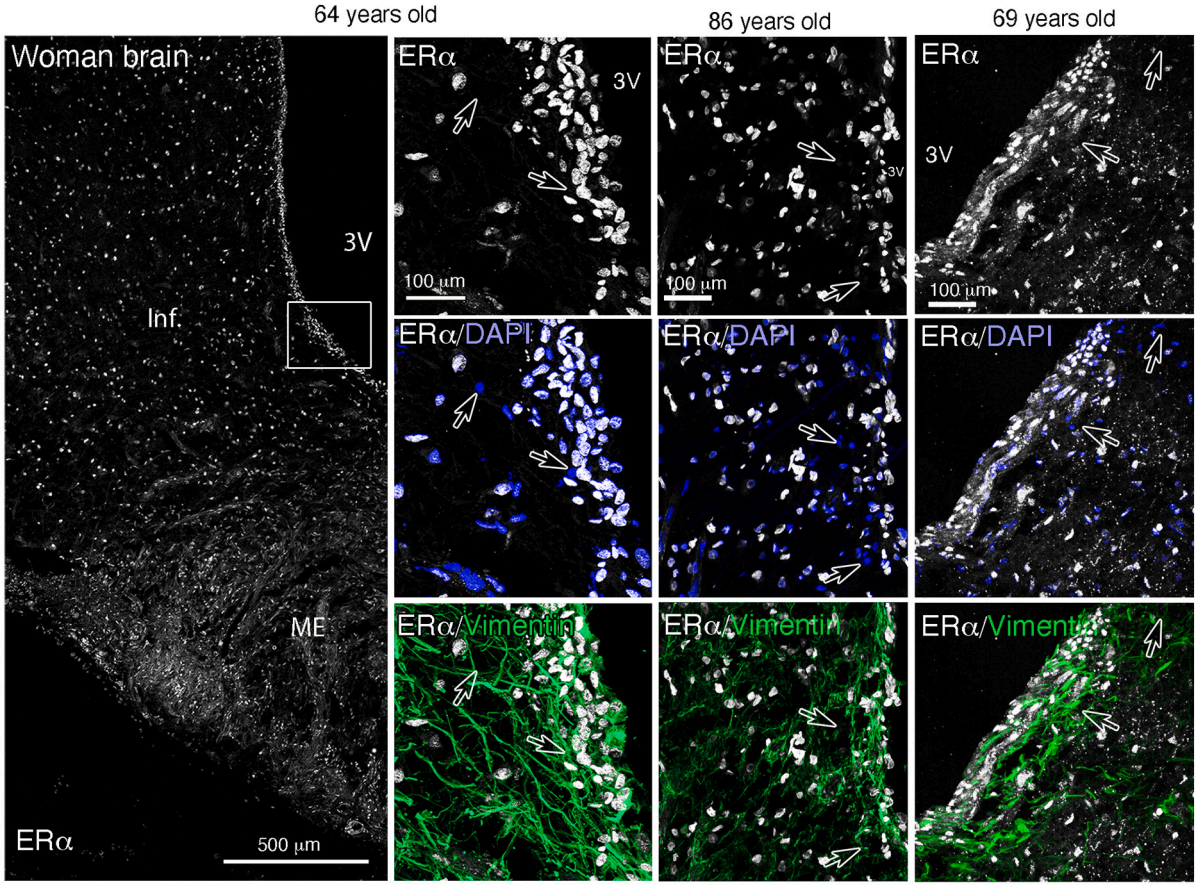

Fig. 6. ERα expression in female tanycytes in the brain of three post-menopausal women. Immunoreactivity for ERα (shown in white) and vimentin (shown in green) in 20-μm thick sections of the hypothalamus from women aged 64, 69 and 86 years. Nuclei were counterstained with DAPI (blue). The panels in the second column depict a higher magnification of the framed region in the corresponding left panel. Empty arrows indicate DAPI-positive nuclei which do not show ERα immunoreactivity. Inf: infundibulum or arcuate nucleus. (For interpretation of the references to colour in this figure legend, the reader is referred to the web version of this article.)

It is known that ARH NPY neurons are activated upon fasting, as indicated by the dramatic induction of cFos expression in these neurons [25,41], and that this phenomenon is blunted by 17β-estradiol treatment [26]. To determine whether tanycytes could be involved in this process, we repeated the experiment in female mice subjected to overnight fasting, with PPT or vehicle treatment administered at food removal. As expected, the fasting-induced high cFos expression in the ventromedial ARH, where NPY neurons are located, was blunted in wildtype mice treated with PTT (Fig. 5C-E). However, in the absence of ERα expression in tanycytes, the PPT-mediated inhibition of fasting-induced cFos expression in the ARH and in arcuate NPY neurons was not only abrogated, but PPT treatment led to a potentiation of fasting-induced cFos immunoreactivity (Fig. 5C-E and Supplementary Fig. 5). Additionally, PPT treatment increased LH pulsatility during fasting (Fig. 5F). Altogether, these results demonstrate that ERα expression in tanycytes is essential for estrogens to exert their anorexigenic effects in the fed state and to suppress the fasting-induced activation of orexigenic ARH NPY neurons, and that these processes in turn influence hormonal outputs that control fertility, including GnRH/LH pulsatile release.

2.6. Tanycytes abundantly express ERα in postmenopausal women

In women at menopause, the permanent arrest of menses following the loss of ovarian follicular growth is accompanied by the suppression of gonadal steroids, including estrogens [42]. Thus, in the absence of estrogen negative feedback to the neural circuits controlling GnRH neuronal activity, the GnRH neuronal network is constantly active, leading to a persistent increase in GnRH/LH pulse frequency or amplitude [43], as also happens after ovariectomy. Postmenopausal women also experience adverse metabolic changes, the risks of which can be reduced by estrogen therapy (see for review [42]). This therapy also normalizes GnRH/LH pulsatility [44]. Our aforementioned pre-clinical results suggest that this process could be mediated by tanycytes. To determine whether female tanycytes also express ERα in humans, we next performed immunofluorescence labeling for ERα in postmortem tissues containing the median eminence from three women aged 64, 69 and 86. The results demonstrated abundant ERα immunoreactivity in the cell nuclei of tanycytes facing the infundibular or arcuate nucleus in postmenopausal women (Fig. 6). In contrast to intact mice (Fig. 3A), the amount of ERα immunoreactivity in tanycytes did not appear to be different from that of neuron-like cells in the parenchyma (Fig. 6).

3. Discussion

The involvement of tanycytes in the control of biological rhythms is becoming increasingly clear both from studies in seasonal species [45–49] and in nonseasonal rodents [33,35,36,50,51]. In the current study, our results shed new light on the involvement of tanycytes in another rhythmic phenomenon: the estrogenic control of pulsatile GnRH/LH release and its coupling with metabolic neuronal circuits in the hypothalamus. We demonstrate that the negative feedback action of gonadal estrogens, which results in restraining GnRH and thus LH pulse frequency and clamping GnRH/LH basal release at low levels, depends on the ability of tanycytes to sense circulating estradiol *via* the

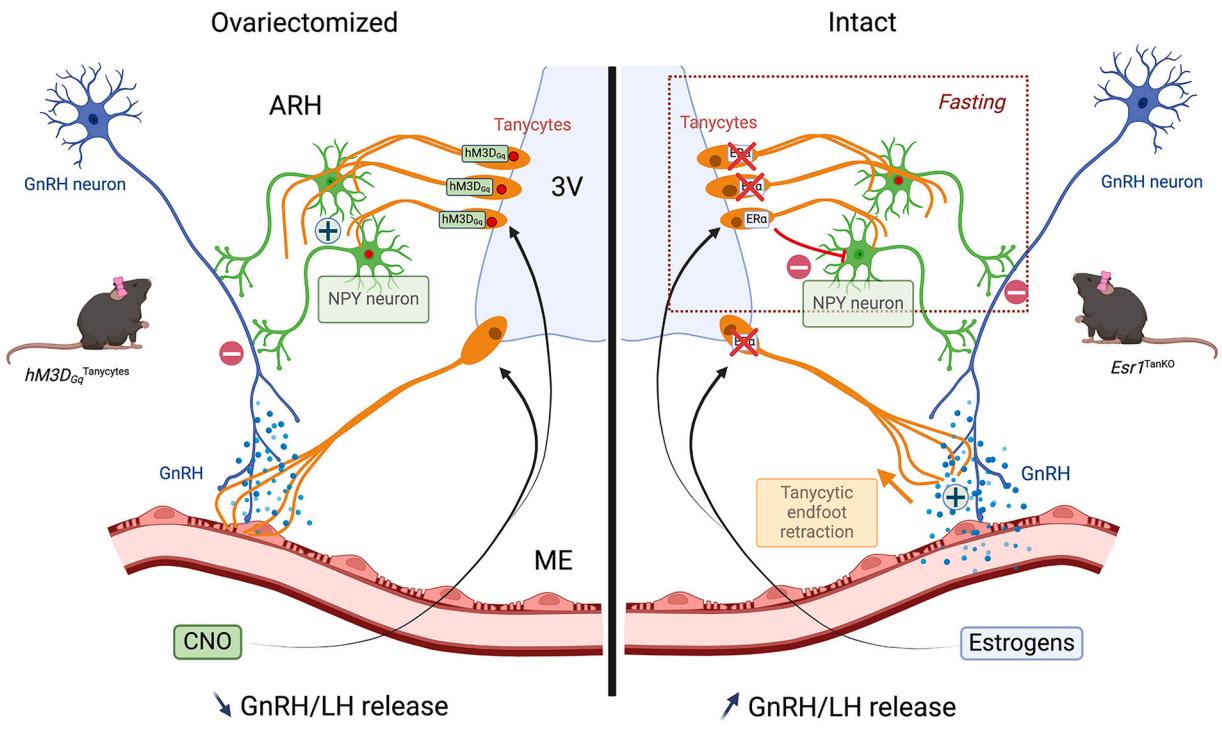

Fig. 7. Tanycyte-neuron interactions in the arcuate nucleus of the hypothalamus (ARH) and the median eminence (ME) at the crossroads of fertility and metabolism. Schematic diagram illustrating tanycyte interactions with NPY neurons in the ARH and GnRH neurons in the median eminence (ME) in ovariectomized (left panel) and intact (right panel) mice in which tanycytes are selectively expressing the activator DREADD (left panel) or deficient in ERα signaling (right panel) in fed or fasting (framed) conditions. Tanycytes play a crucial role in translating the estrogen signal into meaningful information for NPY and GnRH neurons, which rely on this signal for their function but cannot directly detect it. Overall, tanycytes serve as a linchpin in coordinating reproduction and metabolism by perceiving the estrogenic signals and regulating the function of both GnRH and NPY neurons, though additional mechanisms may also be involved. The red circles symbolize cFos expression in cells. CNO, clozapine-N-oxide. Created with BioRender.com. (For interpretation of the references to colour in this figure legend, the reader is referred to the web version of this article.)

expression of ERα and provide this estradiol-weighted information to orexigenic NPY neurons (Fig. 7). While other hypothalamic neuronal populations involved in metabolic regulation do express ERα (see Supplementary Fig. 3, Supplementary Movie 1), including, for example, the anorexigenic POMC neurons of the ARH as well as steroidogenic factor 1 (SF1)-expressing neurons of the ventromedial hypothalamus [52], the mechanism by which estrogenic information is conveyed to orexigenic or appetite-stimulating neurons was unknown until now.

Tanycytes appear to mediate estrogen negative feedback effects on GnRH/LH release in two ways: transmitting these estrogenic signals to NPY/AgRP neurons of the ARH, which control GnRH/LH pulsatile release [21,22,24] but do not themselves express ERα [26] (Supplementary Fig. 3, Supplementary Movie 1), and by directly controlling the access of GnRH neuronal terminals to the pituitary portal circulation in the median eminence [35]. Here we show that estrogen-responsive neuroglial circuits controlling feeding behavior, which include NPY neurons, in turn control the rhythmicity of the reproductive axis. On the flip side, our findings imply that in an environment rich in food, tanycytic estrogen signaling may diminish the drive to eat during specific stages of the estrous cycle, such as in estrus [26]. This could be a strategy to prioritize other behaviors essential for species survival, like seeking a sexual partner and fostering the drive to reproduce.

The peculiar position occupied by tanycytes, at the interface between the peripheral circulation and the cerebrospinal fluid, makes them ideal candidates for the detection and transmission of both blood-borne and brain-generated signals [27,53]. A particular case in point is their ability to translate peripheral information such as glucose levels into signals that neurons that do not express the specific signal-sensing machinery can perceive [31]. Our findings extend this role of tanycytes as molecular interpreters to hypothalamic estrogen sensing, allowing ovarian estrogens to exert their negative feedback on the pattern of GnRH release and thus complete the hypothalamic-pituitary-gonadal circle. While the precise mechanisms involved in the translation of the estrogenic signal by tanycytes of either the ARH or the median eminence remain unknown, *in vivo* and *in vitro* experiments suggest that estrous cyclicity facilitates cytoskeletal remodeling in tanycytes of the median eminence *via* paracrine and autocrine molecular communications, such as PGE_2 production promoting tanycytic endfeet retraction or Sema7a inducing outgrowth [30,36]. Notably, PGE_2 is known to be a potent gliotransmitter in GnRH neurons [54] and possibly in NPY neurons [55], and PGE_2 released by tanycytes has previously been implicated in inflammation-mediated anorexia [56]. Given the anorexigenic effects of estrogens [57,58] and our results in mice lacking ERα in tanycytes suggesting the importance of putative tanycytic gliotransmission to orexigenic AgRP/NPY neurons, which are not only crucial to the regulation of energy homeostasis [59] but can tonically blunt GnRH/LH secretion [21,22,24] and disrupt normal reproductive cycles [23], tanycytes could be the missing link by which gonadal hormones link metabolic state and reproductive function.

Tanycytes had already been seen to transport estrogen from the blood into the brain, and thanks to their striking morphology and suggestive location, had been hypothesized to serve as bridges between the brain and the periphery >50 years ago by pioneers in neuroendocrinology [28]. More recently, the role for tanycytes in energy homeostasis has also been explored, for instance, by ablating tanycytic populations, which leads to alterations in adiposity and insulin resistance, among other effects [60,61]. However, while tanycytes act as transporters for metabolic hormones and signals from the periphery [50,62–67], they also constitute an essential and metabolic-state-responsive blood-cerebrospinal fluid barrier in the median eminence, and such approaches

destroy this barrier and dysregulate the access of peripheral signals to their target neurons and *vice versa*. The more delicate approach we have taken here, activating or inactivating specific cell populations or genetically invalidating ERα specifically in tanycytes without destroying them, or an alternative approach where we have selectively blocked tanycytic vesicular transport *via* the expression of botulinum neurotoxin type B light chain [68], could prove instrumental in teasing apart the intricate mechanisms through which tanycytes mediate hormonal communication between the brain and periphery and the coupling of the reproductive and metabolic axes.

Since we observed abundant ERα immunofluorescence in tanycytes in the infundibular area of the brain of women, one could speculate that tanycytic ERα signaling also plays a role in the control of LH pulsatility and in bridging reproduction and metabolism in humans. In ovariectomized and recently-menopausal women, LH pulses appear to permanently adopt the frequencies seen during the follicular phase, *i.e.* about one pulse every 60 min [43,69]. Interestingly, we observed here that removing ERα in tanycytes accelerates GnRH/LH pulsatility in estrus (the luteal phase, 0–1 pulses/h) to reach a frequency usually seen in diestrus 2 (the follicular phase; 1–2 pulses/h) in mice [10]. A rise in LH pulse frequency due to the loss of tanycytic estradiol signaling in menopausal women may eventually also lead to the loss of viability of GnRH neurons following an initial period of tonic hyperactivity that lasts decades, as suggested by the decrease in GnRH/LH pulsatility with aging [43]. In addition, as circulating estradiol levels decline following menopause, altered ERα signaling between tanycytes and ARH neurons might contribute to weight gain and the increased risk of developing metabolic syndrome in menopausal women [42]. Strengthening the role of estrogens in this process, the use of tamoxifen to antagonize ER function in the context of breast cancer has been reported to promote weight gain, with 48 % of breast cancer survivors treated with tamoxifen developing type 2 diabetes [70]. Finally, GnRH pulsatility has recently been shown to be important for cognitive function as well, including in Alzheimer's disease [71], the incidence of which is higher in women than in men [72,73], with obesity at midlife being a risk factor [74,75]. Intriguingly, tanycytes appear to be degraded in the brain of Alzheimer's patients [76]. All in all, it is tempting to speculate that altered estrogen signaling and GnRH secretion due to the degradation of estrogen-sensing tanycytes may contribute to pathological aging in women.

Taken together, our study demonstrates a new role for tanycytes in transmitting the negative feedback effects of estrogen to the GnRH neuronal network and suggests that ERα signaling in tanycytes could be an interesting target for the prevention of pathological aging in menopausal women, as well as of the undesirable secondary effects of therapies targeting estrogen signaling.

4. Method

4.1. Collection and processing of human tissues

Tissues were obtained following French laws (Good Practice Concerning the Conservation, Transformation and Transportation of Human Tissue to be Used Therapeutically, published on December 29, 1998). Permission to use human tissues was obtained from the French Agency for Biomedical Research (Agence de la Biomedecine, Saint-Denis la Plaine, France, protocol no. PFS16-002) and the Lille Neurobiobank. Dissected blocks of 2 postmenopausal post-mortem women's brains containing the hypothalamus were immersion-fixed in 4 % paraformaldehyde in PBS 0.01 M, pH 7.4 at 4 °C for 1 week. The tissues were cryoprotected in 30 % sucrose/PBS at 4 °C until the fragment sunk, embedded in Tissue-Tek OCT compound (Sakura Finetek), frozen in dry ice and stored at −80 °C until sectioning. Fragments were cut either in coronal or sagittal sections of 20 mm.

4.2. Animals

The study used 77 female mice aged between 9 and 12 weeks from the line Els161 C57BI/6J (*Esr1*$^{loxP/loxP)}$ in which loxP sites were inserted in the exon 3 of the *Esr1* gene. The model has been characterized before [14] and was a generous gift from Pierre Chambon. *Esr1*$^{loxP/loxP}$ mice were mated with td*Tomato*$^{loxP\text{-}STOP\text{-}loxP}$ (Strain# JAX:007914, RRID: IMSR_JAX:007914) to produce the *Esr1*$^{loxP/loxP}$;tdTomato$^{loxP\text{-}STOP\text{-}loxP}$ reporter mice, with *Npy*^{Gfp} mice (JAX stock # 006417) to produce *Npy*^{Gfp};*Esr1*$^{loxP/loxP}$,tdTomato$^{loxP\text{-}STOP\text{-}loxP}$ mice and with the membrane-GFP Cre inducible reporter mouse model *Rosa*^{mTmG} (Strain# JAX007576, RRID:IMSR_JAX:007576) to produce the *Esr1*$^{loxP/loxP}$; *Rosa*^{mTmG} mice. *Esr1*$^{loxP/loxP}$;tdTomato$^{loxP\text{-}STOP\text{-}loxP}$ and *Esr1*$^{+/+}$;tdTomato$^{loxP\text{-}STOP\text{-}loxP}$ littermate mice were used for fluorescence-activated cell sorting (FACS) studies and *Esr1*$^{loxP/loxP}$;*Rosa*^{mTmG} for ERα immunohistochemistry. Additionally, for the chemogenetic activation of tanycytes, we used the ROSA26CAGSloxSTOPloxhMD3$_{Gq}$ (hM3D$_{Gq}^{loxP/loxP}$ mice) female mice aged between 10 and 12 weeks ($N = 6$) generated by inserting hM3D$_{Gq}$ cDNA into the ROSA26 locus carrying a CAGs enhancer element upstream of a loxP-flanked transcriptional STOP-cassette and followed by and IRES-eGFP cassette as previously described [34]. All mice were housed under specific pathogen-free conditions in a temperature-controlled room (21–22 °C) with a 12 h light/dark cycle and *ad libitum* access to food and water. All animal studies were performed with the approval of the Institutional Ethics Committees for the Care and Use of Experimental Animals of the University of Lille and the French Ministry of National Education, Higher Education and Research (APAFIS#2617-2015110517317420 v5), and under the guidelines defined by the European Union Council Directive of September 22, 2010 (2010/63/EU).

4.3. TAT-Cre protein or AAV1/2-Dio2-Cre virus administration

Adult mice were deeply anesthetized with isoflurane (3 % in 1 l/min air flow) in an induction chamber, placed in a stereotaxic apparatus (Kopf Instruments, California) equipped with a mask to maintain anesthesia during the procedure (isoflurane 1 % in 0.7 l/min air flow). Mice were given subcutaneous injections of carprofen (5 mg/kg) after anesthesia was confirmed. Thereafter, a Neurohamilton syringe (Hamilton Company, Ref: 65459-01) hooked to an infusion pump was slowly inserted into the brain third ventricle (coordinates anteroposterior: −1.7 mm, midline: 0 mm and dorsoventral: −5.7 mm from brain) where 2 μl containing 1.27 mg/ml of TAT-Cre fusion protein [77] or 20 mM HEPES, 0.6 M NaCl, pH 7.4 was infused over 10 min as described previously [64]. Alternatively, mice were also stereotaxically administrated in the lateral ventricle (coordinates anteroposterior: −0.3 mm, midline: −1 mm and dorsoventral: −2.5 mm from skull) with 2 μl of AAV1/2-*Dio2*::*Gfp* or AAV1/2-*Dio2*::*Cre* virus (1.25×10^8 vp/μl) over a 10 min period. All stereotaxic coordinates were determined according to Paxinos G. and Watson C Brain mice in stereotaxic coordinates atlas 4th edition [78]. Mice in which a Cre-recombination was carried out in tanycytes are identified as *Esr1*^{TanKO} or hM3D$_{Gq}^{Tanycytes}$; mice injected with vehicle or AAV1/2-*Dio2*::*Gfp* are identified in the manuscript as *Esr1*$^{loxP/loxP}$.

4.4. Study of the estrous cyclicity

The estrous cycle of the mice was determined between 10:00 and 11:00 am daily by a microscopic observation of the cell type present in the vaginal smear as previously described [79]. A fully successful cycle (4–5 days length) was considered when a proestrus was followed by 1 or 2 estrus and then diestrus (we considered diestrus to be both metestrus and diestrus 2). For all the blood sampling and end-point experiments, females were killed in estrus except for FACS experiments in which some mice were also killed in proestrus and diestrus.

4.5. Fertility assessment of adult *Esr1*$^{loxP/loxP}$ mice

Three weeks after stereotaxic surgery, 9 adult virgin *Esr1*$^{loxP/loxP}$ and *Esr1*^{TanKO} female littermates were monitored daily by vaginal cytology for 12 days to characterize estrous cyclicity. Thereafter fertility studies were performed by placing individualized females in diestrus II with an adult wild-type confirmed stud. Pregnancy rate, litter size, gender ratio, and survival percentage were monitored for 75 days. Survival of the offspring was calculated as the percentage of live mice at weaning when compared to the total number of pups at birth of the litter.

4.6. Bi-lateral ovariectomy

Adult mice were deeply anesthetized with isoflurane (3 % in 1 l/min air flow) in an induction chamber, and placed on a surgical table equipped with a mask to maintain anesthesia during the procedure (isoflurane 1 % in 0.7 l/min airflow). Mice were given i.p. injection of carprofen (5 mg/kg) after anesthesia was confirmed. Then a bilateral ovariectomy was performed as described elsewhere [80]. Briefly, ovaries and uterine horns were exteriorized through a dorsal incision in the skin and the ovary, ovarian vessels, ovarian fat, ovarian ligament, and oviduct surrounding the ovary were ligated and cut with the help of an electrocautery. The uterus was replaced inside the general cavity and the muscle and skin were sutured successively. After suture, mice were placed in a clean cage, and body core temperature was maintained at 37 °C with an electrical blanket controlled by a thermostat until mice recovered from the anesthesia. Monitoring of the mice recovery was observed the next morning and afternoon after the surgery. An additional injection of carprofen (5 mg/kg) was performed in mice that presented signs of discomfort the morning after the surgery.

4.7. Isolation of tanycytes cells using fluorescence-activated cell sorting (FACS)

Briefly, *Esr1*$^{loxP/loxP}$;*tdTomato*$^{loxP\text{-}STOP\text{-}loxP}$ (*Esr1*^{TanKO}) and *Esr1*$^{+/+}$;*tdTomato*$^{loxP\text{-}STOP\text{-}loxP}$ (*Esr1*^{Wt}) littermates received a stereotaxic injection of TAT-Cre fusion protein or AAV1/2-Dio2::Cre virus. Three to 4 weeks after, median eminences were microdissected under a magnifier and enzymatically dissociated using a Papain Dissociation System (Worthington, Lakewood, NJ) to obtain a single-cell suspension that was directly used for FACS as described elsewhere [36,64,81]. For immunolabeling of ERα in tomato fluorescent tanycytes, dissociated median eminence cells were fixed in 4 % paraformaldehyde in PBS for 15 min before a permeabilization step with Triton 0.3 % in PBS-2.5 % bovine serum albumin (Sigma-Aldrich). All steps were performed in PBS-BSA 2.5 % and 50 μM EDTA. Cells were incubated with blocking Purified Rat Anti-Mouse CD16/CD32 (553,142, Mouse BD Fc Block™) for 15 min at RT before incubation with primary antibodies anti-ERα (04–820, Millipore) in 10 % Normal Rabbit IgG Control (AB-105-C, R&D Systems) for 1 h at 4 °C, and a following incubation with Goat anti-Rabbit IgG Recombinant Secondary Antibody, Alexa Fluor 647 (Superclonal™A27040, Thermo Scientific) for 1 h at 4 °C. FACS was performed using an ARIA SORP cell sorter cytometer device (BD Bioscience, Inc). The sorting parameters were based on Tomato fluorescence (excitation 561 nm; detection: bandpass 675±20 nm) and Alexa Fluor 647 fluorescence (excitation 633 nm; detection: bandpass 670/30 nm). Autofluorescence was set up by comparing fluorescent median eminence cell suspensions from *Esr1*^{TanKO} and *Esr1*$^{/Wt}$, and cell suspension from the cerebral cortex in which genetic recombination did not occur as illustrated in Fig. 2B and E. For each mouse, a minimum of 1000 tomato-positive and 1000 tomato-negative cells were sorted directly into 10 μl of lysis buffer containing 0.1 % Triton® X-100 and 0.4 unit/μl RNaseOUT™ (10777019, Invitrogen™).

4.8. Quantitative real time PCR analyses

Briefly, 4000 to 1000 FACS-sorted tomato-positive and tomato-negative cells were reverse transcribed using High-capacity cDNA Reverse transcription kit (4368814, Applied Biosystems™) after a DNAse treatment (18068015, DNase I, Amplification Grade, Invitrogen™). For FACS-collected cells, before real-time PCR a linear pre-amplification step was performed using the TaqMan® PreAmp Master Mix Kit (4488593, Applied Biosystems™). Next, real-time PCR was carried out on Applied Biosystems 7900HT Fast Real-Time PCR System using the TaqMan™ Universal Master Mix II (4440049, Applied Biosystems™) and the TaqMan® probes: *Esr1* (Mm00433149_m1) and *Esr2* (Mm00599821_m1). *Npy* (Mm01410146_m1), *Agrp* (Mm00475829_g1), *Pomc* (Mm00435874_m1), *Cartpt* (Mm04210469_m1). Control housekeeping genes *18S* (Mm03928990_g1), *Gapdh* (Mm99999915_g1) and *Actb* (Mm00607939_s1) were used for analysis. Gene expression data were analyzed using the $2^{-\Delta\Delta Ct}$ method. At least 2 housekeeping genes were tested for each sample analyzed.

4.9. Tail-tip bleeding for LH measurements

Tail-tip blood sampling was undertaken as described before [10]. Briefly, a small cut was made in the tip of the tail, and 3 μl of whole blood was taken every 6 min in ovariectomized mice and every 10 min in intact females and immediately diluted into 60 μl of 0.01 M PBS pH 7.4 with 0.05 % Tween 20, vortexed and stored at −80 °C until the day of the LH ELISA assay. Mice were habituated to daily handling for at least 2 weeks before blood collection.

4.10. LH and ovarian steroids quantification

A well-established ultrasensitive ELISA was used to measure circulating LH levels [10,82,83]. Briefly, 96-well high-affinity binding plates (CLS3369, Corning®) were coated with a bovine LHβ518B7 monoclonal antibody (1:1000 in PBS; 50 μl per well). Circulating hormone levels were determined using a mouse LH-RP reference provided by Albert F. Parlow (National Hormone & Pituitary Program, Torrance, CA, USA). A rabbit polyclonal primary antibody for LH (1:10,000; rabbit antiserum AFP240580Rb; National Hormone and Peptide Program, USA) and a polyclonal goat anti-rabbit IgG secondary antibody (1:1000 PI-1000, Vector Laboratories) were used in this assay. Intra- and inter-assay variations were 8 % and 12 % respectively. The commercially available mouse estradiol (DE2693, Demeditec Diagnostics, GmnH) and progesterone (DEV9988, Demeditec Diagnostics, GmnH) kits were used to measure gonadal steroids following the manufacturer's instructions. For progesterone, we used as a positive control the kit DEV99RC (Demeditec Diagnostics, GmnH).

4.11. Immunohistochemistry

All female adult mice were killed in the morning of estrus. Mice were intracardially perfused with 4 % paraformaldehyde in PBS 0.01 M pH 7.4. The brains were harvested and post-fixed in the same fixative solution overnight. Thereafter, brains were cryoprotected in 30 % sucrose-Tris buffer (TBS 0.01 M pH 7.4), frozen in dry ice, and cut into three series of 40-μm thick coronal sections using a stage cryomicrotome (Leica®, Germany). For immunolabeling of mice (free-floating brain sections) and human (20-μm thick sections collected on glass slides using a cryostat) brain sections were incubated after tawing and being rinsed three times in TBS 0.01 M pH 7.4 and blocked for 1 h in 0.4 % Triton-0.1%BSA in TBS 0.01 M pH 7.4 with: rabbit polyclonal antibody anti-ERα (1:500, 06-935 Millipore), rabbit polyclonal antibody cFos (1:1000 623_2018_SA90 82-1, Synaptic systems or cFos (9F6) #2250 Rabbit monoclonal antibody, Cell Signaling), chicken polyclonal antibody anti-vimentin (1:1000, AB5733, Sigma-Aldrich) and rabbit polyclonal antibody anti-GFP (Rabbit 1:1000 A6455, Invitrogen,

ThermoFisher Scientific or Chicken 1:1000 GFP-1020, AvesLabs) in incubation solution (ICS: 0.4 % Triton-0.1%BSA in TBS 0.01 M pH 7.4) with 10 % normal donkey serum for 48 h at 4 °C under mild agitation. Brain sections were washed 4 times per 10 min in TBS before secondary antibodies incubation. In brief, sections were incubated in a mix of the corresponding secondary antibodies (1:500 Invitrogen, ThermoFisher Scientific Donkey Anti-Rabbit IgG (H + L), Alexa Fluor™ 488, Alexa Fluor™ 568, and Alexa Fluor™ 647 ref. A21206, A100042 and A31573 respectively and 1:500, Jackson ImmunoResearch Laboratories Inc. Donkey Anti-Chicken Alexa Fluor® 4 Alexa and Fluor® 594 ref: 703-545-155 and 703-585-155 respectively). All secondary antibodies were diluted in ICS and incubated with sections for 2 h at room temperature. For ERα immunolabeling detection in tanycytes of mice, a step of tyramide amplification was carried out according to the manufacturer's instruction (SAT700001EA, TSA biotin Reagent AKOYA Biosciences). Nuclei were counterstained by incubating sections with DAPI (1:5000 D9542, Sigma Aldrich) for 10 min at RT. All labelled sections were mounted onto superfrost glass slides. For human hypothalamus immunolabeling, a citrate-buffer antigen retrieval step, 10 mM Citrate in TBS-Triton 0.1 % pH 6 for 30 min at 70 °C, was performed on 20-μm cryostat-cut sections. After 3 washes of 5 min with TBS-Triton 0.1 %, sections were blocked in incubation solution (ICS2: 10 % normal donkey serum, 1 mg/ml BSA in TBS-Triton 0.1 % pH 7,4) for 1 h. Blocking was followed with primary antibody incubation rabbit polyclonal antibody anti-ERα (1:250, 06-935, Millipore) and chicken polyclonal antibody anti-vimentin (1:1.000, AB5733, Sigma-Aldrich) in ICS2 for 48 h at 4 °C. Primary antibodies were then rinsed out, before incubation in fluorophore-coupled secondary antibodies for 1 h in ICS2 at room temperature. Secondary antibodies were washed and sections were counterstained with DAPI (1:5.000 Sigma ref.: D9542). Finally, sections were treated with Autofluorescence Eliminator Reagent (Merck Millipore ref.:2610) to quench lipofuscin aggregates autofluorescence before being coverslipped with Mowiol.

4.12. Fluorescent in situ hybridization (RNAScope)

RNA-fluorescent *in situ* hybridization (FISH) was performed on 40-μm thick brain free-floating coronal sections containing the tuberal region of the hypothalamus in mice perfused with 4 % paraformaldehyde, 0.01 M PBS pH 7.4 as described before with the RNAscope® Multiplex Fluorescent Kit v2 to detect *Esr1* (478201-C3, NM_007956.5 Target Region: 678–1723), *Fos* (316921-C2, NM_010234.2 Target Region: 407–1427) and *Npy* (313321, NM_023456.2 Target Region: 28–548) mRNAs. For *Esr1* FISH was coupled to immunohistochemistry using the chicken polyclonal antibody anti-vimentin (1:1000, AB5733, Sigma-Aldrich). FISH was performed according to the manufacturer's instructions, with some modifications for free-floating sections as described before by others [84]. Hybridization with a probe against the *Bacillus subtilis* dihydrodipicolinate reductase (dapB) gene was used as a negative control.

4.13. Image acquisition

Image acquisition was performed using an inverted confocal microscope (LSM 710, Zeiss, Jena, Germany), Leica Stellaris 5, Leica Microsystems, Germany, and Axio Imager.Z2 ApoTome (Zeiss, Jena, Germany). Excitation/emission wavelengths of 493/562 nm, 568/643 and 640/740 were selected to image Alexa-488, Alexa-568, Alexa-647 secondary antibodies for the immunohistochemistry. TSA plus Fluorescein, Cyanine-3 and Cyanine-5 were imaged at 493/562 nm, 568/643 and 640/740 for FISH. UV laser (wavelength of 355 nm) was used to image DAPI. Z-stack images were acquired with a W Plan-APOCHROMAT 20× objective (NA 0.5, zoom 1.0), HC PL FLUOTAR 10×/0.30 DRY (NA 0.3, zoom 1.0), and high-magnification photomicrographs were acquired with a 63× objective (NA 1.4). Images for figures were merged using Photoshop v23.3.2 (Adobe Systems, San Jose, CA).

4.14. Electron microscopy and GnRH immunolabeling

Mice were decapitated and the brain was quickly harvested with the pituitary attached to the brain. Blocks of hypothalamic explants containing the median eminence were microdissected using razor blades. Explants were then processed for electron microscopy as described previously [35,85]. Briefly, tissues were fixed by immersion in a solution of 2 % paraformaldehyde, 0.2 % picric acid and 0.1 % glutaraldehyde in 0.1 M phosphate buffer, pH 7.4, over-night at 4 °C. Tissues were post-fixed with 1 % OsO4 in phosphate buffer for 1 h at RT. After dehydration, tissues were embedded in Araldite. Semithin sections (1–2 μm thick) were used to progressively approach and identify the portion of the median eminence targeted for ultrastructural studies, that is, the area where the pituitary stalk becomes distinct from the base of the hypothalamus but remains attached to it by the hypophyseal portal vasculature [35]. This area, which does not extend beyond 20 μm, contains high numbers of GnRH fibers. To detect GnRH immunoreactivity, ultrathin sections (80–90 nm thick) collected on Parlodion 0.8 %/isoamyl acetate-coated 100 mesh grids (EMS, Fort Washington, PA) were treated using an immunogold procedure described previously [35,85]. Briefly, after a preliminary treatment with H_2O_2 (10 %, 8 min) and a blocking step in TBS (0.1 M Tris, pH 7.4, 0.15 M NaCl) containing 1 % normal goat serum and 1 % bovine albumin serum (10 min at RT), the grids were floated on a drop of the following reagents and washing solutions: (1) rabbit anti-GnRH (1:5000; a generous gift from Prof. Tramu) in bovine albumin serum for 60 h at 4 °C, (2) TBS to remove excess antibodies (three times for 10 min), (3) colloidal gold (18 nm)-labelled goat anti-rabbit immunoglobulins (111–215-144, Jackson ImmunoResearch) 1:20 in TBS for 90 min at RT, (4) TBS (three times for 10 min) and (5) distilled water (three times for 10 min). The sections were then counterstained with uranyl acetate and lead citrate before observation. The specificity of the GnRH antisera used has been discussed previously [35,85]. Ultrathin immunolabelled sections were examined with a Zeiss transmission electron microscope 902 (Leo, Rueil-Malmaison, France) and images were acquired using a Gatan Orius SC1000 CCD camera (Gatan France, Grandchamp, France). The morphometric analysis was performed by an experimenter blind to the hypothalamic explant treatment on digitalized images taken at an original magnification of x12,000 from 10 to 15 ultrathin sections per animal. All GnRH-immunoreactive nerve terminals located at <8 μm from the parenchymatous basal lamina (that is, the pial surface of the brain) were taken into consideration, that is, >100 distinct axon terminals per animals (that is, almost all GnRH nerve terminals abutting onto the pituitary portal blood vessels in the 20-μm-thick region of the median eminence). Immunolabelled terminals confined to 10 μm or less from the basal lamina were imaged and the distance from the nerve terminal and the pericapillary space recorded. The number of immunoreactive GnRH terminals confined to <1 μm from the basal lamina was then counted for each animal and multiplied by 100 to obtain the percentage of GnRH terminals contacting the basal lamina in each treatment condition. Electron microscopic analyses were performed in 3- to 5-month-old estrus *Esr1*$^{loxP/loxP}$ and *Esr1*^{TanKO} mice, and *Esr1*$^{loxP/loxP}$ 15 days after ovariectomy.

4.15. Ovarian morphology

Immediately after sacrifice, the right ovaries of the mice were set in Bouin's fixative solution post-fixed overnight at 4C, and then stored in 70 % ethanol until paraffin embedding. Ovarian sections of 5 μm thickness were collected and stained with hematoxylin–eosin. All slices were analyzed and preantral, antral follicles, and corpora lutea were counted and measured. The classification criteria of the follicular structures were performed according to previous studies [86,87]. In brief, primordial follicles were counted when the oocyte was surrounded

by the sample flattened squamous epithelium, corresponding to the follicular granulosa cells. Primary follicles were identified when the oocyte is surrounded by a single layer of cuboidal granulosa cells, secondary follicles when at least 2 layers of cuboidal granulosa cells are present. Antral follicles were defined as follicles with an antral cavity and with 2 or more layers of granulosa cells. Atretic follicles were defined as those in which >5 % of the cells had pyknotic nuclei in the largest cross-section and showed shrinkage and an occasional breakdown of the germinal vesicle. All follicles were counted and measured when the nucleus of the oocyte was visualized. Corpora lutea were analyzed in every section and they were included for counting when the corpus luteum reaches the largest cross-section. For every follicle two cross-sectional diameters were obtained from basement membrane to basement membrane. Images were captured using x20 objectives on the NanoZoomer Digital Pathology Scanner (Hamamatsu 470 Photonics). Quantification was realized on each 4th section in the NDP View2 software.

4.16. CNO/hM3D$_{Gq}$ activation protocol

Five adult ovariectomized *hM3D*$_{Gq}^{Tanycytes}$ mice between 9 and 11 weeks were subjected to a 1 h tail-tip blood sampling for LH measurement as described above. Thereafter all mice received an intraperitoneal injection of 1 mg/kg clozapine-N-oxide (CNO) (Tocris/Bio-Techne ref.:63295) and were subjected to iterative bleeding for 1 extra hour. The total iterative bleeding period was of 2 h as illustrated in Fig. 1A. In parallel, height *hM3D*$_{Gq}^{loxP\text{-}STOP\text{-}loxP}$ mice were subjected to fasting for 2 h during the light phase (food was removed 3 h after lights on). After this time, mice were injected intraperitoneally with a single dose of 1 mg/kg (CNO). Food was reintroduced into the cage and weighed 2 h later. The same batch of mice were then injected intracerebroventricularly with AAV1/2-*Dio2*::*Cre* to induce hM3DGq receptor expression in tanycytes. Two weeks later, *hM3D*$_{Gq}^{Tanycytes}$ mice were again subjected to a 2 h fasting and subsequent intraperitoneal injection of CNO (1 mg/kg), and food intake was assessed 2 h after refeeding.

4.17. Food intake assessment in mice treated with the ERα agonist

Female mice were placed in individual cages. Mice were injected at lights off with 100*u*l of DMSO 0.1 % in sesame oil and the other half 100 µl of 5 mM of 4,4′,4″-(4-Propyl-[1H]-pyrazole-1,3,5-triyl)trisphenol (PPT), a potent selective ERα agonist (Tocris Bioscience, Cat. 1426) [40] resuspended in DMSO 0.1 % and placed in sesame oil. One group of mice had free access to food overnight and food consumption was assessed at lights on (Fig. 5A). In another group, food was removed at lights off and mice were subjected to overnight fasting (12*h*); food was reintroduced at lights on and food consumption was measured every hour for 4 h and at 10 h (Fig. 5B).

4.18. Indirect calorimetry in mice

One week post-ovariectomy, mice were individually housed and allowed to acclimate to their cages for 48 h. The study was conducted within a 12 h light/dark cycle (with lights on from 08:00 to 20:00 h) in a room maintained at a controlled temperature 22 ± 1 °C. At 18:00 h, all mice received a subcutaneous injection of 100 ul of sesame oil for two consecutive days, followed by daily injections of estradiol benzoate (1 µg/100 µl/mouse. Sigma-Aldrich Cat. *E8515*) for three consecutive days. We measured energy expenditure, oxygen consumption, carbon dioxide production and food intake using calorimetric cages (Labmaster, TSE Systems GmbH). Fatty acid oxidation was calculated as described before [51] based on energy expenditure, and respiratory exchange ratio. Throughout the experiment, mice were monitored daily for changes in body weight.

4.19. Quantification of cFos-positive cells

hM3D$_{Gq}^{Tanycytes}$ mice were injected with Saline (VH) or 1 mg/kg CNO (CNO) 30 min before being perfusion-fixed as detailed above. Quantitative analyses were performed on two FISH-processed 40-µm thick brain sections containing the ARH (between coordinate −1.6 mm and -2 mm from bregma) for each mouse. Cells positive for *Fos* and *Npy* transcripts and cells in which the two transcripts colocalized were counted on confocal images captured from both sides using the Software Zen2.3 blue edition (Carl Zeiss Microscopy GmbH, 2011).

Twelve-hour overnight fasting *Npy*::*Gfp*;*Esr1*$^{loxP/loxP}$ and *Npy*::*Gfp*;*Esr1*^{TanKO} mice were injected subcutaneously with vehicle (VH; 100 µl DMSO 0.1 % in sesame oil) or 5 mM PPT (100ul DMSO 0.1 % in sesame oil) at lights off and subjected to intracardiac perfusion with the fixative solution 12 h after at lights on. Quantitative analyses were performed on nine to ten immunofluorescent-processed 40-µm thick brain sections containing the ARH (between coordinate −1.2 mm and −2.8 mm from bregma) for each mouse. Cells immunoreactive for cFos and cells showing GFP fluorescence, as well as cells in which cFos immunoreactivity and GFP fluorescence colocalized, were counted on confocal images captured from both sides using semi-automatic Quanty-cFos, ImageJ/Fiji Algorithm [88].

4.20. Statistical analysis

Statistical analysis was performed with the PRISM software v9.3.1 (GraphPad Software, San Diego, CA, USA). Normal distribution was determined with D'Agostino-Pearson's or Shapiro-Wilk normality test. Statistical analyses were performed using paired or unpaired Student *t*-test when corresponding, or one- way ANOVA followed by a Fisher's LSD *post hoc* test. All data are presented as mean ± standard error of the media (SEM). A P value of <0.05 was considered statistically significant. All tests performed were two-tailed. Statistically significant differences are indicated by asterisks, * for $p < 0.05$, ** for $p < 0.01$, *** for $p < 0.001$ and **** for $p < 0.0001$.

Supplementary data to this article can be found online at https://doi.org/10.1016/j.metabol.2024.155976.

CRediT authorship contribution statement

Daniela Fernandois: Writing – original draft, Methodology, Investigation, Formal analysis, Data curation, Conceptualization. **Mariam Rusidzé:** Investigation. **Helge Mueller-Fielitz:** Methodology. **Eleonora Deligia:** Investigation. **Mauro S.B. Silva:** Methodology, Investigation. **Florence Evrard:** Investigation. **Aurelio Franco-García:** Formal analysis. **Daniele Mazur:** Investigation. **Ines Martinez-Corral:** Investigation. **Nathalie Jouy:** Methodology. **S. Rasika:** Writing – review & editing. **Claude-Alain Maurage:** Resources, Methodology. **Paolo Giacobini:** Investigation. **Ruben Nogueiras:** Methodology, Investigation. **Benedicte Dehouck:** Investigation. **Markus Schwaninger:** Methodology, Formal analysis. **Francoise Lenfant:** Resources, Methodology, Funding acquisition. **Vincent Prevot:** Writing – review & editing, Supervision, Methodology, Investigation, Funding acquisition, Conceptualization.

Declaration of competing interest

The authors declare no competing interests.

Data availability

The authors confirm that all data are available in the main text or the Supplementary materials.

Acknowledgments

The authors would like to thank Jens Brüning (Max Planck Institute for Metabolism Research, Cologne, Germany) for the kind gift of the $hM3D_{Gq}^{loxP/loxP}$ mice and PLBS UAR 2014 – US41 (https://ums-plbs.univ-lille.fr/) with its different platforms and staff for expert technical assistance: Meryem Tardivel and Antonino Bongiovanni (microscopy core facility, BICeL) and Julien Devassine (Animal house) for expert technical assistance. Funding. This work was supported by the European Research Council (ERC) Synergy Grant WATCH No. 810331 to R. N., V. P. and M.S. and the Agence Nationale de la Recherche (ANR-18-CE14-0002 to F.L. and V.P.). D.F. received a postdoctoral fellowship from the Fondation pour la Recherche Médicale (FRM grant No. AMI202112015388). A.F-G. received "Ayuda para la Formación de Profesorado Universitario" program of MICINN (FPU19/01722).

References

[1] Hunzicker-Dunn M, Mayo K. Gonadotropinsignaling in the ovary. In: Plant TM, Zeleznik J, editors. Knobil and Neill's physiology of reproduction. 4th ed. New York: Elsevier; 2015. p. 895–946.
[2] Sarkar DK, Minami S. Diurnal variation in luteinizing hormone-releasing hormone and beta-endorphin release in pituitary portal plasma during the rat estrous cycle. Biol Reprod 1995;53:38–45.
[3] Frost SI, Keen KL, Levine JE, Terasawa E. Microdialysis methods for in vivo neuropeptide measurement in the stalk-median eminence in the Rhesus monkey. J Neurosci Methods 2008;168:26–34.
[4] Caraty A, Orgeur P, Thiery JC. Demonstration of the pulsatile secretion of LH-RH into hypophysial portal blood of ewes using an original technic for multiple samples. C R Sci Acad Sci III 1982;295:103–6.
[5] Clarke IJ, Cummins JT. The temporal relationship between gonadotropin releasing hormone (GnRH) and luteinizing hormone (LH) secretion in ovariectomized ewes. Endocrinology 1982;111:1737–9.
[6] Moenter SM, Brand RC, Karsch FJ. Dynamics of gonadotropin-releasing hormone (GnRH) secretion during the GnRH surge: insights into the mechanism of GnRH surge induction. Endocrinology 1992;130:2978–84.
[7] Moenter SM, Brand RM, Midgley AR, Karsch FJ. Dynamics of gonadotropin-releasing hormone release during a pulse. Endocrinology 1992;130:503–10.
[8] Hoffman AR, Crowley Jr WF. Induction of puberty in men by long-term pulsatile administration of low-dose gonadotropin-releasing hormone. N Engl J Med 1982; 307:1237–41.
[9] Reame N, Sauder SE, Kelch RP, Marshall JC. Pulsatile gonadotropin secretion during the human menstrual cycle: evidence for altered frequency of gonadotropin-releasing hormone secretion. J Clin Endocrinol Metab 1984;59:328–37.
[10] Czieselsky K, Prescott M, Porteous R, Campos P, Clarkson J, Steyn FJ, et al. Pulse and surge profiles of luteinizing hormone secretion in the mouse. Endocrinology 2016;157:4794–802.
[11] Wintermantel TM, Campbell RE, Porteous R, Bock D, Grone HJ, Todman MG, et al. Definition of estrogen receptor pathway critical for estrogen positive feedback to gonadotropin-releasing hormone neurons and fertility. Neuron 2006;52:271–80.
[12] Wang L, Vanacker C, Burger LL, Barnes T, Shah YM, Myers MG, et al. Genetic dissection of the different roles of hypothalamic kisspeptin neurons in regulating female reproduction. Elife 2019:8.
[13] Mayer C, Acosta-Martinez M, Dubois SL, Wolfe A, Radovick S, Boehm U, et al. Timing and completion of puberty in female mice depend on estrogen receptor alpha-signaling in kisspeptin neurons. Proc Natl Acad Sci U S A 2010;107:22693–8.
[14] Dupont S, Krust A, Gansmuller A, Dierich A, Chambon P, Mark M. Effect of single and compound knockouts of estrogen receptors alpha (ERalpha) and beta (ERbeta) on mouse reproductive phenotypes. Development 2000;127:4277–91.
[15] d'Anglemont de Tassigny X, Campagne C, Dehouck B, Leroy D, Holstein GR, Beauvillain JC, et al. Coupling of neuronal nitric oxide synthase to NMDA receptors via postsynaptic density-95 depends on estrogen and contributes to the central control of adult female reproduction. J Neurosci 2007;27:6103–14.
[16] Chachlaki K, Malone SA, Qualls-Creekmore E, Hrabovszky E, Munzberg H, Giacobini P, et al. Phenotyping of nNOS neurons in the postnatal and adult female mouse hypothalamus. J Comp Neurol 2017;525:3177–89.
[17] Cheong RY, Czieselsky K, Porteous R, Herbison AE. Expression of ESR1 in glutamatergic and GABAergic neurons is essential for normal puberty onset, estrogen feedback, and fertility in female mice. J Neurosci 2015;35:14533–43.
[18] Wakabayashi Y, Nakada T, Murata K, Ohkura S, Mogi K, Navarro VM, et al. Neurokinin B and dynorphin A in kisspeptin neurons of the arcuate nucleus participate in generation of periodic oscillation of neural activity driving pulsatile gonadotropin-releasing hormone secretion in the goat. J Neurosci 2010;30: 3124–32.
[19] Dubois SL, Acosta-Martinez M, DeJoseph MR, Wolfe A, Radovick S, Boehm U, et al. Positive, but not negative feedback actions of estradiol in adult female mice require estrogen receptor alpha in kisspeptin neurons. Endocrinology 2015;156:1111–20.
[20] McQuillan HJ, Clarkson J, Kauff A, Han SY, Yip SH, Cheong I, et al. Definition of the estrogen negative feedback pathway controlling the GnRH pulse generator in female mice. Nat Commun 2022;13:7433.
[21] Woller MJ, Terasawa E. Estradiol enhances the action of neuropeptide Y on in vivo luteinizing hormone-releasing hormone release in the ovariectomized rhesus monkey. Neuroendocrinology 1992;56:921–5.
[22] Vulliemoz NR, Xiao E, Xia-Zhang L, Wardlaw SL, Ferin M. Central infusion of agouti-related peptide suppresses pulsatile luteinizing hormone release in the ovariectomized rhesus monkey. Endocrinology 2005;146:784–9.
[23] Padilla SL, Qiu J, Nestor CC, Zhang C, Smith AW, Whiddon BB, et al. AgRP to Kiss1 neuron signaling links nutritional state and fertility. Proc Natl Acad Sci U S A 2017; 114:2413–8.
[24] Coutinho EA, Prescott M, Hessler S, Marshall CJ, Herbison AE, Campbell RE. Activation of a classic hunger circuit slows luteinizing hormone pulsatility. Neuroendocrinology 2020;110:671–87.
[25] Ichimaru T, Mori Y, Okamura H. A possible role of neuropeptide Y as a mediator of undernutrition to the hypothalamic gonadotropin-releasing hormone pulse generator in goats. Endocrinology 2001;142:2489–98.
[26] Olofsson LE, Pierce AA, Xu AW. Functional requirement of AgRP and NPY neurons in ovarian cycle-dependent regulation of food intake. Proc Natl Acad Sci U S A 2009;106:15932–7.
[27] Prevot V, Dehouck B, Sharif A, Ciofi P, Giacobini P, Clasadonte J. The versatile tanycyte: a hypothalamic integrator of reproduction and energy metabolism. Endocr Rev 2018;39:333–68.
[28] Kumar TC, Knowles F. A system linking the third ventricle with the pars tuberalis of the rhesus monkey. Nature 1967;215:54–5.
[29] Langub Jr MC, Watson Jr RE. Estrogen receptor-immunoreactive glia, endothelia, and ependyma in guinea pig preoptic area and median eminence: electron microscopy. Endocrinology 1992;130:364–72.
[30] de Seranno S, d'Anglemont de Tassigny X, Estrella C, Loyens A, Kasparov S, Leroy D, et al. Role of estradiol in the dynamic control of tanycyte plasticity mediated by vascular endothelial cells in the median eminence. Endocrinology 2010;151:1760–72.
[31] Lhomme T, Clasadonte J, Imbernon M, Fernandois D, Sauve F, Caron E, et al. Tanycytic networks mediate energy balance by feeding lactate to glucose-insensitive POMC neurons. J Clin Invest 2021;131:e140521.
[32] Bolborea M, Pollatzek E, Benford H, Sotelo-Hitschfeld T, Dale N. Hypothalamic tanycytes generate acute hyperphagia through activation of the arcuate neuronal network. Proc Natl Acad Sci U S A 2020;117:14473–81.
[33] Muller-Fielitz H, Stahr M, Bernau M, Richter M, Abele S, Krajka V, et al. Tanycytes control the hormonal output of the hypothalamic-pituitary-thyroid axis. Nat Commun 2017;8:484.
[34] Steculorum SM, Ruud J, Karakasilioti I, Backes H, Engstrom Ruud L, Timper K, et al. AgRP neurons control systemic insulin sensitivity via myostatin expression in brown adipose tissue. Cell 2016;165:125–38.
[35] Prevot V, Croix D, Bouret S, Dutoit S, Tramu G, Stefano GB, et al. Definitive evidence for the existence of morphological plasticity in the external zone of the median eminence during the rat estrous cycle: implication of neuro-glio-endothelial interactions in gonadotropin-releasing hormone release. Neuroscience 1999;94:809–19.
[36] Parkash J, Messina A, Langlet F, Cimino I, Loyens A, Mazur D, et al. Semaphorin7A regulates neuroglial plasticity in the adult hypothalamic median eminence. Nat Commun 2015;6:6385.
[37] Weidlinger S, Winterberger K, Pape J, Weidlinger M, Janka H, von Wolff M, et al. Impact of estrogens on resting energy expenditure: a systematic review. Obes Rev 2023;24:e13605.
[38] Camporez JP, Jornayvaz FR, Lee HY, Kanda S, Guigni BA, Kahn M, et al. Cellular mechanism by which estradiol protects female ovariectomized mice from high-fat diet-induced hepatic and muscle insulin resistance. Endocrinology 2013;154: 1021–8.
[39] Ainslie DA, Morris MJ, Wittert G, Turnbull H, Proietto J, Thorburn AW. Estrogen deficiency causes central leptin insensitivity and increased hypothalamic neuropeptide Y. Int J Obes Relat Metab Disord 2001;25:1680–8.
[40] Harris HA, Katzenellenbogen JA, Katzenellenbogen BS. Characterization of the biological roles of the estrogen receptors, ERalpha and ERbeta, in estrogen target tissues in vivo through the use of an ERalpha-selective ligand. Endocrinology 2002; 143:4172–7.
[41] Munzberg H, Jobst EE, Bates SH, Jones J, Villanueva E, Leshan R, et al. Appropriate inhibition of orexigenic hypothalamic arcuate nucleus neurons independently of leptin receptor/STAT3 signaling. J Neurosci 2007;27:69–74.
[42] Davis SR, Lambrinoudaki I, Lumsden M, Mishra GD, Pal L, Rees M, et al. Menopause. Nat Rev Dis Primers 2015;1:15004.
[43] Hall JE, Lavoie HB, Marsh EE, Martin KA. Decrease in gonadotropin-releasing hormone (GnRH) pulse frequency with aging in postmenopausal women. J Clin Endocrinol Metab 2000;85:1794–800.
[44] Rossmanith WG, Handke-Vesely A, Wirth U, Scherbaum WA. Does the gonadotropin pulsatility of postmenopausal women represent the unrestrained hypothalamic-pituitary activity? Eur J Endocrinol 1994;130:485–93.
[45] Melum VJ, Saenz de Miera C, Markussen FAF, Cazarez-Marquez F, Jaeger C, Sandve SR, et al. Hypothalamic tanycytes as mediators of maternally programmed seasonal plasticity. Curr Biol 2024;34:632–640.e6 [in press].
[46] Rivagorda M, Prevot V, Schwaninger M. Seasonal plasticity: tanycytes give the hypothalamus a spring makeover. Curr Biol 2024;34:R209–11. in press.
[47] Saenz de Miera C, Bothorel B, Jaeger C, Simonneaux V, Hazlerigg D. Maternal photoperiod programs hypothalamic thyroid status via the fetal pituitary gland. Proc Natl Acad Sci U S A 2017;114:8408–13.
[48] Samms RJ, Lewis JE, Lory A, Fowler MJ, Cooper S, Warner A, et al. Antibody-mediated inhibition of the FGFR1c isoform induces a catabolic lean state in Siberian hamsters. Curr Biol 2015;25:2997–3003.

[49] Yamamura T, Hirunagi K, Ebihara S, Yoshimura T. Seasonal morphological changes in the neuro-glial interaction between gonadotropin-releasing hormone nerve terminals and glial endfeet in Japanese quail. Endocrinology 2004;145:4264–7.
[50] Rodriguez-Cortes B, Hurtado-Alvarado G, Martinez-Gomez R, Leon-Mercado LA, Prager-Khoutorsky M, Buijs RM. Suprachiasmatic nucleus-mediated glucose entry into the arcuate nucleus determines the daily rhythm in blood glycemia. Curr Biol 2022;32:796–805e4.
[51] Imbernon M, Dehouck B, Prevot V. Glycemic control: tanycytes march to the beat of the suprachiasmatic drummer. Curr Biol 2022;32:R173–6.
[52] Xu Y, Nedungadi TP, Zhu L, Sobhani N, Irani BG, Davis KE, et al. Distinct hypothalamic neurons mediate estrogenic effects on energy homeostasis and reproduction. Cell Metab 2011;14:453–65.
[53] Nampoothiri S, Nogueiras R, Schwaninger M, Prevot V. Glial cells as integrators of peripheral and central signals in the regulation of energy homeostasis. Nat Metab 2022;4:813–25.
[54] Clasadonte J, Poulain P, Hanchate NK, Corfas G, Ojeda SR, Prevot V. Prostaglandin E2 release from astrocytes triggers gonadotropin-releasing hormone (GnRH) neuron firing via EP2 receptor activation. Proc Natl Acad Sci U S A 2011;108:16104–9.
[55] Varela L, Stutz B, Song JE, Kim JG, Liu ZW, Gao XB, et al. Hunger-promoting AgRP neurons trigger an astrocyte-mediated feed-forward autoactivation loop in mice. J Clin Invest 2021;131.
[56] Bottcher M, Muller-Fielitz H, Sundaram SM, Gallet S, Neve V, Shionoya K, et al. NF-kappaB signaling in tanycytes mediates inflammation-induced anorexia. Mol Metab 2020;39:101022.
[57] Gao Q, Mezei G, Nie Y, Rao Y, Choi CS, Bechmann I, et al. Anorectic estrogen mimics leptin's effect on the rewiring of melanocortin cells and Stat3 signaling in obese animals. Nat Med 2007;13:89–94.
[58] Eckel LA. The ovarian hormone estradiol plays a crucial role in the control of food intake in females. Physiol Behav 2011;104:517–24.
[59] Yeo GSH, Chao DHM, Siegert AM, Koerperich ZM, Ericson MD, Simonds SE, et al. The melanocortin pathway and energy homeostasis: from discovery to obesity therapy. Mol Metab 2021;48:101206.
[60] Rohrbach A, Caron E, Dali R, Brunner M, Pasquettaz R, Kolotuev I, et al. Ablation of glucokinase-expressing tanycytes impacts energy balance and increases adiposity in mice. Mol Metab 2021;53:101311.
[61] Yoo S, Cha D, Kim S, Jiang L, Cooke P, Adebesin M, et al. Tanycyte ablation in the arcuate nucleus and median eminence increases obesity susceptibility by increasing body fat content in male mice. Glia 2020;68:1987–2000.
[62] Balland E, Dam J, Langlet F, Caron E, Steculorum S, Messina A, et al. Hypothalamic tanycytes are an ERK-gated conduit for leptin into the brain. Cell Metab 2014;19:293–301.
[63] Collden G, Balland E, Parkash J, Caron E, Langlet F, Prevot V, et al. Neonatal overnutrition causes early alterations in the central response to peripheral ghrelin. Mol Metab 2015;4:15–24.
[64] Duquenne M, Folgueira C, Bourouh C, Millet M, Silva A, Clasadonte J, et al. Leptin brain entry via a tanycytic LepR-EGFR shuttle controls lipid metabolism and pancreas function. Nat Metab 2021;3:1071–90.
[65] Imbernon M, Saponaro C, Helms HCC, Duquenne M, Fernandois D, Deligia E, et al. Tanycytes control hypothalamic liraglutide uptake and its anti-obesity actions. Cell Metab 2022;34:1054–63e7.
[66] Pena-Leon V, Folgueira C, Barja-Fernandez S, Perez-Lois R, Da Silva Lima N, Martin M, et al. Prolonged breastfeeding protects from obesity by hypothalamic action of hepatic FGF21. Nat Metab 2022;4:901–17.
[67] Porniece Kumar M, Cremer AL, Klemm P, Steuernagel L, Sundaram S, Jais A, et al. Insulin signalling in tanycytes gates hypothalamic insulin uptake and regulation of AgRP neuron activity. Nat Metab 2021;3:1662–79.
[68] Duquenne M, Deligia E, Folgueira C, Bourouh C, Caron E, Pfrieger F, et al. Tanycytic transcytosis inhibition disrupts energy balance, glucose homeostasis and cognitive function in male mice. Mol Metab 2024 [in press].
[69] Grana-Barcia M, Lado-Abeal J, Liz-Leston JL, Lojo S, Novo-Dominguez A, Aguilar-Fernandez J. Depression of FSH and LH secretion following pulsatile GnRH administration in ovariectomized women. Hum Reprod 1998;13:525–30.
[70] Hamood R, Hamood H, Merhasin I, Keinan-Boker L. Diabetes after hormone therapy in breast cancer survivors: a case-cohort study. J Clin Oncol 2018;36:2061–9.
[71] Manfredi-Lozano M, Leysen V, Adamo M, Paiva I, Rovera R, Pignat JM, et al. GnRH replacement rescues cognition in down syndrome. Science 2022;377:eabq4515.
[72] Demetrius LA, Eckert A, Grimm A. Sex differences in Alzheimer's disease: metabolic reprogramming and therapeutic intervention. Trends Endocrinol Metab 2021;32:963–79.
[73] Sauve F, Kacimi L, Prevot V. The hypothalamic-pituitary-gonadal axis and the enigma of Alzheimer disease sex differences. Nat Rev Endocrinol 2024. https://doi.org/10.1038/s41574-024-00981-1.
[74] Livingston G, Huntley J, Sommerlad A, Ames D, Ballard C, Banerjee S, et al. Dementia prevention, intervention, and care: 2020 report of the Lancet Commission. Lancet 2020;396:413–46.
[75] Fitzpatrick AL, Kuller LH, Lopez OL, Diehr P, O'Meara ES, Longstreth Jr WT, et al. Midlife and late-life obesity and the risk of dementia: cardiovascular health study. Arch Neurol 2009;66:336–42.
[76] Sauvé F, Ternier G, Dewisme J, Lebouvier T, Dupré E, Danis D, et al. Tanycytes are degraded in Alzheimer's Disease, disrupting the brain-to-blood efflux of Tau. medRxiv; 2022. https://doi.org/10.1101/2022.05.04.22274181.
[77] Peitz M, Pfannkuche K, Rajewsky K, Edenhofer F. Ability of the hydrophobic FGF and basic TAT peptides to promote cellular uptake of recombinant Cre recombinase: a tool for efficient genetic engineering of mammalian genomes. Proc Natl Acad Sci U S A 2002;99:4489–94.
[78] Paxinos G, Franklin KBJ. The mouse brain in stereotaxic coordinates. London: Academic Press; 2004.
[79] Cora MC, Kooistra L, Travlos G. Vaginal cytology of the laboratory rat and mouse: review and criteria for the staging of the estrous cycle using stained vaginal smears. Toxicol Pathol 2015;43:776–93.
[80] Stout Steele M, Bennett RA. Clinical technique: dorsal ovariectomy in rodents. J Exotic Pet Med 2011;20:222–6.
[81] Langlet F, Levin BE, Luquet S, Mazzone M, Messina A, Dunn-Meynell AA, et al. Tanycytic VEGF-A boosts blood-hypothalamus barrier plasticity and access of metabolic signals to the arcuate nucleus in response to fasting. Cell Metab 2013;17:607–17.
[82] Steyn FJ, Wan Y, Clarkson J, Veldhuis JD, Herbison AE, Chen C. Development of a methodology for and assessment of pulsatile luteinizing hormone secretion in juvenile and adult male mice. Endocrinology 2013;154:4939–45.
[83] Silva MSB, Desroziers E, Hessler S, Prescott M, Coyle C, Herbison AE, et al. Activation of arcuate nucleus GABA neurons promotes luteinizing hormone secretion and reproductive dysfunction: implications for polycystic ovary syndrome. EBioMedicine 2019;44:582–96.
[84] Grabinski TM, Kneynsberg A, Manfredsson FP, Kanaan NM. A method for combining RNAscope in situ hybridization with immunohistochemistry in thick free-floating brain sections and primary neuronal cultures. PloS One 2015;10:e0120120.
[85] Prevot V, Dutoit S, Croix D, Tramu G, Beauvillain JC. Semi-quantitative ultrastructural analysis of the localization and neuropeptide content of gonadotropin releasing hormone nerve terminals in the median eminence throughout the estrous cycle of the rat. Neuroscience 1998;84:177–91.
[86] Cruz G, Barra R, González D, Sotomayor-Zárate R, Lara HE. Temporal window in which exposure to estradiol permanently modifies ovarian function causing polycystic ovary morphology in rats. Fertil Steril 2012;98:1283–90.
[87] Fernandois D, Lara HE, Paredes AH. Blocking of β-adrenergic receptors during the subfertile period inhibits spontaneous ovarian cyst formation in rats. Horm Metab Res 2012;44:682–7.
[88] Beretta CA, Liu S, Stegemann A, Gan Z, Wang L, Tan LL, et al. Quanty-cFOS, a novel ImageJ/Fiji algorithm for automated counting of Immunoreactive cells in tissue sections. Cells 2023:12.